Droop-free Distributed Control for AC Microgrids

Nasirian, Vahidreza ; Shafiee, Qobad; Guerrero, Josep M.; L. Lewis, Frank ; Davoudi, Ali

Published in:
I E E E Transactions on Power Electronics

DOI (link to publication from Publisher):
10.1109/TPEL.2015.2414457

Publication date:
2016

Document Version
Early version, also known as pre-print

Droop-free Distributed Control for AC Microgrids

Vahidreza Nasirian, *Student Member, IEEE*, Qobad Shafiee, *Student Member, IEEE*, Josep M. Guerrero, *Senior Member, IEEE*, Frank L. Lewis, *Fellow, IEEE*, and Ali Davoudi, *Member, IEEE*

Abstract

A cooperative distributed secondary/primary control paradigm for AC microgrids is proposed. This solution replaces the centralized secondary control and the primary-level droop mechanism of each inverter with three separate regulators: voltage, reactive power, and active power regulators. A sparse communication network is spanned across the microgrid to facilitate limited data exchange among inverter controllers. Each controller processes its local and neighbors' information to update its voltage magnitude and frequency (or, equivalently, phase angle) set points. A voltage estimator finds the average voltage across the microgrid, which is then compared to the rated voltage to produce the first voltage correction term. The reactive power regulator at each inverter compares its normalized reactive power with those of its neighbors, and the difference is fed to a subsequent PI controller that generates the second voltage correction term. The controller adds the voltage correction terms to the microgrid rated voltage (provided by the tertiary control) to generate the local voltage magnitude set point. The voltage regulators collectively adjust the average voltage of the microgrid at the rated voltage. The voltage regulators allow different set points for different bus voltages and, thus, account for the line impedance effects. Moreover, the reactive power regulators adjust the voltage to achieve proportional reactive load sharing. The third module, the active power regulator, compares the local normalized active power of each inverter with its neighbors' and uses the difference to update the frequency and, accordingly, the phase angle of that inverter. The global dynamic model of the microgrid, including distribution grid, regulator modules, and the communication network, is derived, and controller design guidelines are provided. Steady-state performance analysis shows that the proposed controller can accurately handle the global voltage regulation and proportional load sharing. An AC microgrid prototype is set up, where the controller performance, plug-and-play capability, and resiliency to the failure in the communication links are successfully verified.

***Index Terms*— AC microgrids, Cooperative control, Distributed control, Droop control, Inverters**

This work was supported in part by the National Science Foundation under grants ECCS-1137354 and ECCS-1405173 and in part by the U.S. Office of Naval Research under grant N00014-14-1-0718. Vahidreza Nasirian, Frank L. Lewis, and Ali Davoudi are with the Department of Electrical Engineering, University of Texas, Arlington, TX 76019 USA and are also with the University of Texas at Arlington Research Institute (UTARI), Fort Worth, TX 76118 USA (emails: vahidreza.nasirian@mavs.uta.edu; lewis@uta.edu; davoudi@uta.edu). Qobad Shafiee and Josep M. Guerrero are with the Department of Energy Technology, Aalborg University, Denmark. Qobad Shafiee was also on leave with the University of Texas, Arlington, TX (qsh@et.aau.dk; joz@et.aau.dk).

I. Introduction

Microgrids are small-scale power systems that can island from the legacy grid. They have gained popularity in distribution systems for their improved efficiency, reliability, and expandability [1]–[6]. DC energy resources, e.g., photovoltaic arrays, storage elements, and fuel cells, are commonly connected to the AC microgrid distribution network via voltage-source inverters [7], [8]. A three-tier hierarchical control structure is conventionally adopted for the microgrid operation [9], [10]. The primary control, usually realized through a droop mechanism, operates on a fast timescale and regulates inverters' output voltage and handles proportional load sharing among inverters [9]. It shares the total load demand among sources in proportion to their power ratings and is commonly practiced to avoid overstressing and aging of the sources [7]–[9]. The secondary control, in an intermediate timescale, compensates for the voltage and frequency deviations caused by the primary control by updating inverter voltage set points [11]–[13]. Ultimately, the tertiary control carries out the scheduled power exchange with the main grid over a longer timescale [14], [15].

Droop mechanism, or its variations [16]–[27], is a common decentralized approach to realize the primary control, although alternative methods (e.g., virtual oscillator control [28]–[31]) are emerging. They emulate virtual inertia for AC systems and mimic the role of governors in traditional synchronous generators [32]. Despite simplicity, the droop mechanisms suffers from 1) load-dependent frequency/voltage deviation, 2) poor performance in handling nonlinear loads [33], and 3) poor reactive power sharing in presence of unequal bus voltages [34]. Unequal bus voltages are indispensible in practical systems to perform the scheduled reactive power flow. Droop techniques cause voltage and frequency deviations and, thus, a supervisory secondary control is inevitable to update the set points of the local primary controls [35]–[40]. For example, GPS-coordinated time referencing handles frequency synchronization across the microgrid in [33], [38], [39]. Such architecture requires two-way high bandwidth communication links between the central controller and each inverter. This protocol adversely affects the system reliability as failure of any communication link hinders the functionality of the central controller and, thus, the entire microgrid. The central controller itself is also a reliability risk since it imposes a single point-of-failure. Scalability is another issue for that it adds to the complexity of the communication network and it requires updating the settings of the central controller.

Spatially dispersed inverter-based microgrids naturally lend themselves to distributed control techniques to address their synchronization and coordination requirements. Distributed control architectures can discharge duties of a central controller while being resilient to faults or unknown system parameters. Distributed synchronization processes necessitate that each agent (i.e., the inverter) exchange information with other agents according to some restricted communication protocol [5], [41], [42]. These controllers can use a sparse communication network and have less computational complexity at each inverter controller [43]. Networked control of parallel inverters in [44], [45] embeds the functionality of the secondary control in all inverters, i.e.,

it requires a fully connected communication network. The master node in the networked master-slave methods [46]–[48] is still a single point-of-failure. Distributed cooperative control is recently introduced for AC [49]–[51] and DC microgrids [52]–[55]. Distributed control of AC microgrids are also discussed in [56]–[58] (using a ratio-consensus algorithm), [50] (a multi-objective approach), and [59]-[62] (using a distributed averaging proportional controller). Majority of such approaches are still based on the droop mechanism (and, thus, inherit its shortcoming), require system information (e.g., number of inverters, inverter parameters, and total load demand), require frequency measurement, and mainly handle active power sharing and frequency regulation (or, only reactive power sharing/voltage control). Recent works of the authors in [50] and [51] investigate distribution networks with negligible line impedances and, potentially, can lack satisfactory performance in practical multi-terminal distribution systems with intricate and lossy transmission networks. They also assign a single source as *leader*, who relays the rated frequency and voltage set points to other sources through a communication network. Moreover, such solutions focus on the islanded mode of operation and their extension to grid-connected mode is not straightforward.

This paper provides a comprehensive distributed cooperative solution that satisfies both the secondary and the primary control objectives for an autonomous AC microgrid without relying on the droop mechanism. Herein, each inverter is considered as an agent of a multi-agent system (i.e., the microgrid); each inverter exchanges data with a few other neighbor inverters and processes the information to update its local voltage set points and synchronize their normalized power and frequencies. The proposed controller includes three modules: voltage regulator, reactive power regulator, and active power regulator. The salient features of the proposed control method are:

- Cooperation among inverters on a communication graph provides two voltage correction terms to be added to the rated voltage and adjust the local voltage set points of individual inverters.
- Cooperation among voltage, reactive power, and active power regulators effectively carries out global voltage regulation, frequency synchronization, and proportional load sharing, particularly, in practical networks where the transmission/ distribution line impedances are not negligible.
- Normally, the controllers share the total load among sources in proportion to their rated active and reactive powers; however, the rated values, embedded in the controller, can be manipulated to achieve any desired load sharing.
- The voltage regulator seeks to adjust the average voltage across the microgrid, rather than the individual inverter busses, at the rated voltage value, and ensures global voltage regulation without the need to run a power flow analysis.
- The control method does not employ any droop mechanism and does not require any frequency measurement.
- The proposed scheme does not require prior knowledge of system parameters or the number of inverters. Thus, it features scalability, modularity, robustness (independent of loads), and plug-and-play capability.

- Only a sparse communication graph is sufficient for the limited message passing among inverters. This is in direct contrast with the centralized control approaches that require high-bandwidth bidirectional communication networks, or existing networked control techniques that require fully-connected communication graphs.

The rest of this paper is outlined as follows: Section II discusses the proposed control methodology. Section III provides dynamic/static model of the entire microgrid including the physical distribution grid, control modules, and communication network, and shows that the controller objectives are also met in the steady state. The controller performance is experimentally verified using an AC microgrid prototype in Section IV. Section V concludes the paper.

II. Proposed Cooperative Control Framework

A. *Microgrid as a Cyber-physical System*

A distribution network is an electric network that provides the physical connection between sources and loads within a microgrid. Such a physical system can be equipped with a cyber network to exploit different control opportunities. Interaction of the sources (i.e., inverter-augmented DC sources) in the cyber domain offers cooperative decision making, which features scalability and improves reliability. Here, a microgrid is assumed to be cyber-physical system with a communication network that facilitates data exchange among sources for control and monitoring purposes. Figure 1(a) illustrates physical and cyber layers of the microgrid. Each source broadcasts its information, e.g., voltage and power measurements, to a few selected sources, called its *neighbors*. As oppose to the centralized/supervisory control, this communication layout forms a sparse network; not all sources need to communicate.

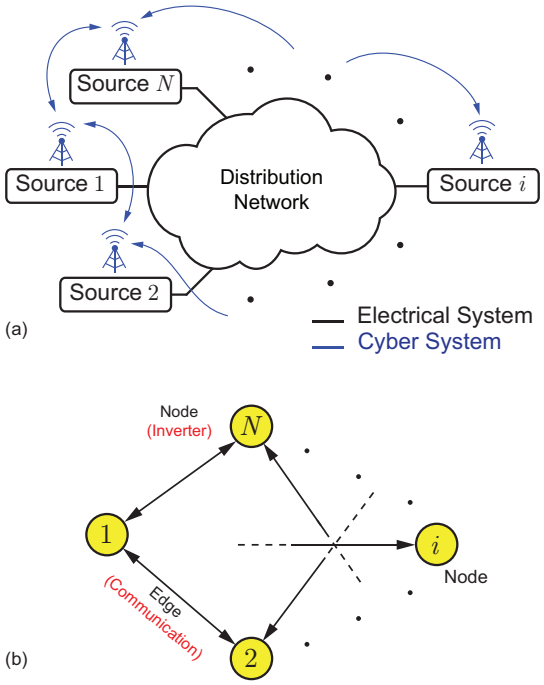

Fig. 1. General layout of an AC microgrid: (a) Sources supplying the grid with communication infrastructure spanned across the grid, (b) Graphical representation of the cyber-physical system.

From the control perspective, a multi-agent cyber-physical system can be expressed with a graphical representation with active agents (sources) modeled as nodes of the graph and communication links mapped to edges connecting nodes (see Fig. 1(b)). Communication links may not be reciprocal, forming a directed graph (digraph). Each node and edge inherit the dynamic model of the corresponding agent and communication channel, respectively. Information links may exchange data with

different gains referred to as the *communication weights*. For example, if Node j broadcasts data x_j to Node i through a link with designated a weight of $a_{ij} > 0$, then, the information received at node i is $a_{ij}x_j$. Generally, $a_{ij} > 0$ if Node i receives data from Node j and $a_{ij} = 0$, otherwise. Such a graph is usually represented by an associated adjacency matrix $\mathbf{A_G} = \left[a_{ij}\right] \in \mathbb{R}^{N\times N}$ that carries the communication weights, where N is the number of dispatchable sources. Communication weights can be time varying and may include some channel delay; however, this study assumes time-invariant and scalar adjacency matrix. N_i denotes the set of all neighbors of Node i. The in-degree and out-degree matrices $\mathbf{D}^{\text{in}} = \text{diag}\left\{d_i^{\text{in}}\right\}$ and $\mathbf{D}^{\text{out}} = \text{diag}\left\{d_i^{\text{out}}\right\}$ are diagonal matrices with $d_i^{\text{in}} = \sum_{j\in N_i} a_{ij}$ and $d_i^{\text{out}} = \sum_{i\in N_j} a_{ji}$, respectively. The Laplacian matrix is defined as $\mathbf{L} \triangleq \mathbf{D}^{\text{in}} - \mathbf{A_G}$, whose eigenvalues determine the global dynamics of the entire system (i.e., the microgrid) [63], [64]. The Laplacian matrix is balanced if the in-degree and out-degree matrices are equal; particularly, an undirected (bidirectional) data network satisfies this requirement. A direct path from Node i to Node j is a sequence of edges that connects the two nodes. A digraph is said to have a spanning tree if it contains a root node, from which, there exists at least a direct path to every other node. Here, a graph is called to carry the *minimum redundancy* if it contains enough redundant links that, in the case of any single link failure, it remains connected and presents a balanced Laplacian matrix.

B. Proposed Cooperation Policy

The proposed method requires a communication graph with the adjacency matrix $\mathbf{A_G} = \left[a_{ij}\right] \in \mathbb{R}^{N\times N}$ that 1) has at least a spanning tree, 2) can be undirected or directional, yet with a balanced Laplacian matrix, and 3) the graph must carry the minimum redundancy. Communication weights, a_{ij}, are design parameters. Each source exchanges a vector of information, $\Psi_i = \left[\overline{e}_i, p_i^{\text{norm}}, q_i^{\text{norm}}\right]$, with its neighbor sources on the communication graph, where $\overline{e}_i$ is the estimation of the averaged voltage magnitude across the microgrid, processed at Node i. $p_i^{\text{norm}} \triangleq p_i \big/ p_i^{\text{rated}}$ and $q_i^{\text{norm}} \triangleq q_i \big/ q_i^{\text{rated}}$ are the normalized active and reactive powers supplied by Source i. p_i and q_i are the measured active and reactive powers supplied by Source i, respectively, and p_i^{rated} and q_i^{rated} are the rated active and reactive powers of the same source. The control strategy attempts to share the load among sources in proportion to their rated powers.

Objectives of the secondary/primary controller are 1) global voltage regulation, 2) frequency synchronization, 3) active power sharing, and 4) reactive power sharing. Generally, fine adjustment of the voltage magnitude and frequency can satisfy all four objectives. Particularly, active and reactive power flow can be managed by tuning the frequency and voltage magnitude, respectively. The proposed control method is established on this notion. Figure 2 shows the schematic of the control policy for Node i (Source i). The controller consists of three separate modules: the voltage regulator, reactive power regulator, and active power regulator.

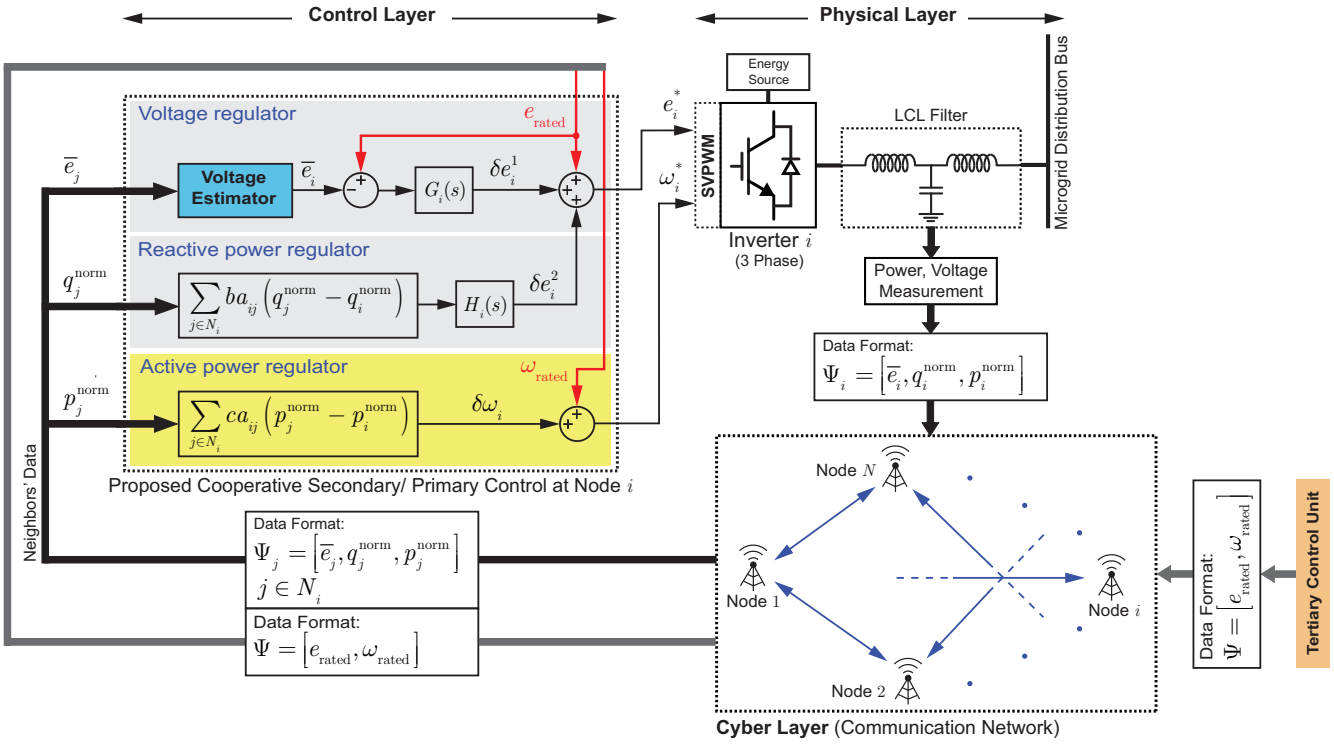

Fig. 2. Proposed cooperative secondary control for the Source i, of the AC microgrid. Note data exchange with the neighbor nodes.

The controller at Node i receives information vectors of its neighbors, Ψ_js, and processes the neighbors' and local data, Ψ_i, to update its voltage set point. e_i^* and ω_i^* are the set points of the (line to neutral) voltage magnitude (rms value) and frequency, respectively. Accordingly, the Space Vector PWM (SVPWM) module generates the actual voltage set point, v_i^*,

$$v_i^*(t) = e_i^*(t)\sqrt{2}\sin\left(\int_0^t \omega_i^*(\tau)\mathrm{d}\tau\right), \tag{1}$$

and assigns appropriate switching signals to drive the inverter module [65]. It should be noted that the controller is assumed activated at $t=0$. As seen in Fig. 2, each inverter is followed by an LCL filter to attenuate undesired (switching and line-frequency) harmonics. The set point in (1) is the reference voltage for the output terminal of the filtering module or, equivalently, the microgrid bus that corresponds to Source i.

The voltage and reactive power regulator modules adjust the set point of the voltage magnitude by producing two voltage correction terms, δe_i^1 and δe_i^2, respectively, as

$$e_i^*(t) = e_{\text{rated}} + \delta e_i^1(t) + \delta e_i^2(t), \tag{2}$$

where e_{rated} is the rated voltage magnitude of the microgrid. Regardless of the operating mode, i.e., islanded or grid-connected modes, the rated voltage can be safely assumed equal for all active nodes (dispatchable sources). The voltage regulator at Node i includes an estimator that finds the global averaged voltage magnitude, i.e., the averaged voltage across the microgrid. This

estimation is, then, compared with the rated voltage, e_{rated}, and the difference is fed to a PI controller, G_i, to generate the first voltage correction term, δe_i^1, and, thus, handle global voltage regulation. Accordingly, the voltage regulators collectively adjust the average voltage of the microgrid on the rated value, yet individual bus voltages may slightly deviate from the rated value (typically, less than 5%). This deviation is essential in practice to navigate reactive power across the microgrid. Therefore, the reactive power regulator at Node i adjusts an additional (i.e., the second) voltage correction term, δe_i^2, to control the supplied reactive power. This module calculates the neighborhood reactive loading mismatch, mq_i,

$$mq_i = \sum_{j\in N_i} ba_{ij}(q_j^{\text{norm}} - q_i^{\text{norm}}), \tag{3}$$

which measures how far is the normalized reactive power of the Source i from the average of its neighbors'. The coupling gain b is a design parameter. The mismatch in (3) is then fed to a PI controller, H_i, (see Fig. 2) to adjust the second voltage correction term, δe_i^2, and, accordingly, mitigate the mismatch. Performance analysis in Section III-E will show that all the mismatch terms, in the steady state, converge to zero and, thus, all normalized reactive powers would synchronize. This satisfies the proportional reactive power sharing among sources.

The active power regulator at Source i controls its frequency and active power. This module calculates the neighborhood active loading mismatch to assign the frequency correction term, $\delta\omega_i$,

$$\delta\omega_i = \sum_{j\in N_i} ca_{ij}(p_j^{\text{norm}} - p_i^{\text{norm}}), \tag{4}$$

where the coupling gain c is a design parameter. As seen in Fig. 2, this correction term is added to the rated frequency, ω_{rated},

$$\omega_i^*(t) = \omega_{\text{rated}} + \delta\omega_i(t), \tag{5}$$

and, thus, (1) can be written as

$$v_i^*(t) = e_i^*(t)\sqrt{2}\sin\left(\omega_{\text{rated}}t + \int_0^t \delta\omega_i \mathrm{d}\tau\right). \tag{6}$$

Equation (6) helps to define the phase angle set point for Source i,

$$\delta_i^*(t) \triangleq c\int_0^t \sum_{j\in N_i} a_{ij}(p_j^{\text{norm}} - p_i^{\text{norm}})\,\mathrm{d}\tau. \tag{7}$$

According to (6)–(7), the active power regulator module keeps the frequency at the rated value and fine tunes the phase angle set point, δ_i^*, to reroute the active power across the microgrid and mitigate the neighborhood active loading mismatch. It is shown in Section III-E that all phase angles, δ_i^*, will converge to their steady-state values and, thus, all frequency correction terms, $\delta\omega_i$, decay to zero. Therefore, the microgrid frequency synchronizes to the rated frequency, ω_{rated}, without any frequency measurement loop, while the controller stabilizes the phase angles, δ_i. Indeed, transient variations in the inverter

frequency adjust its phase angle and control the active power flow; the frequency will not deviate from the rated value in the steady state and normalized active powers will synchronize, which provides the proportional active load sharing.

The proposed controller is a general solution that can handle load sharing for variety of distribution systems; i.e., predominantly inductive, inductive-resistive, or primarily resistive networks. Indeed, the nature of the line impedances defines the role of the active and reactive power regulators (see Fig. 2) for load sharing. In particular, a predominantly inductive network naturally decouples the load sharing process; the reactive power regulator must handle the reactive load sharing by adjusting voltage magnitude while the active power regulator would handle the active load sharing through adjusting the frequency (or, equivalently, the phase angle). However, for other types of distribution network, active and reactive power flows are entangled to both voltage and phase angle adjustment. For such cases, the load sharing is a collaborative task where the two regulators (i.e., both the active and reactive power regulators) would work together to generate the desired set points.

The proposed controller, so far, assumes fixed and known power rating for dispatchable sources. In a scenario that some sources are non-dispatchable, i.e., renewable energy sources with stochastic power output, the proposed controller can be augmented with the methodology shown in Fig. 3. Supplied power by each stochastic source is measured and reported to an auxiliary control unit. This module runs optimization scenarios, e.g., Maximum Power Point Tracking (MPPT), to decide the desired operating points. It also compares the desired generation with the actual supplied power and updates the rated powers, p_i^{rated} and q_i^{rated}, to address any mismatch. The proposed control routine in Fig. 2 uses the tuned rated powers to adjust the voltage and frequency set points. With the modification in Fig. 3, the stochastic sources will be pushed to exploit their potentials (e.g., to produce maximum power) while the controller in Fig. 2 proportionally shares the remaining load demand among dispatchable sources.

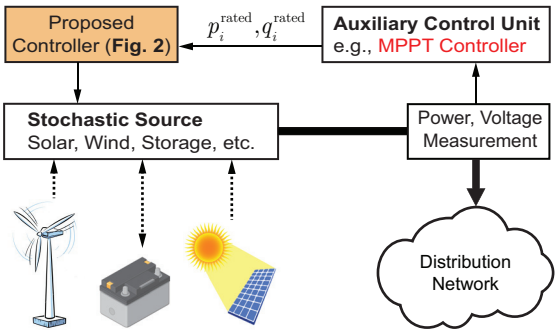

Fig. 3. Extension of the proposed controller to non-dispatchable (e.g., stochastic) energy sources.

In the islanded mode, the system operational autonomy requires preset (fixed) values for the rated voltage magnitude and frequency, e_{rated} and ω_{rated}, in all controllers. The voltage and frequency settings typically follow the standard ratings of the nearby electricity grid. To further extend operational range of the proposed controller to the grid-connected mode, one can consider adjustable voltage magnitude and frequency ratings. To this end, a tertiary controller (highlighted in Fig. 2) fine-tunes such ratings. There is a single tertiary controller for the entire microgrid, and it uses the same communication network as the secondary controllers, to propagate updated voltage and frequency ratings to all secondary controllers across the microgrid.

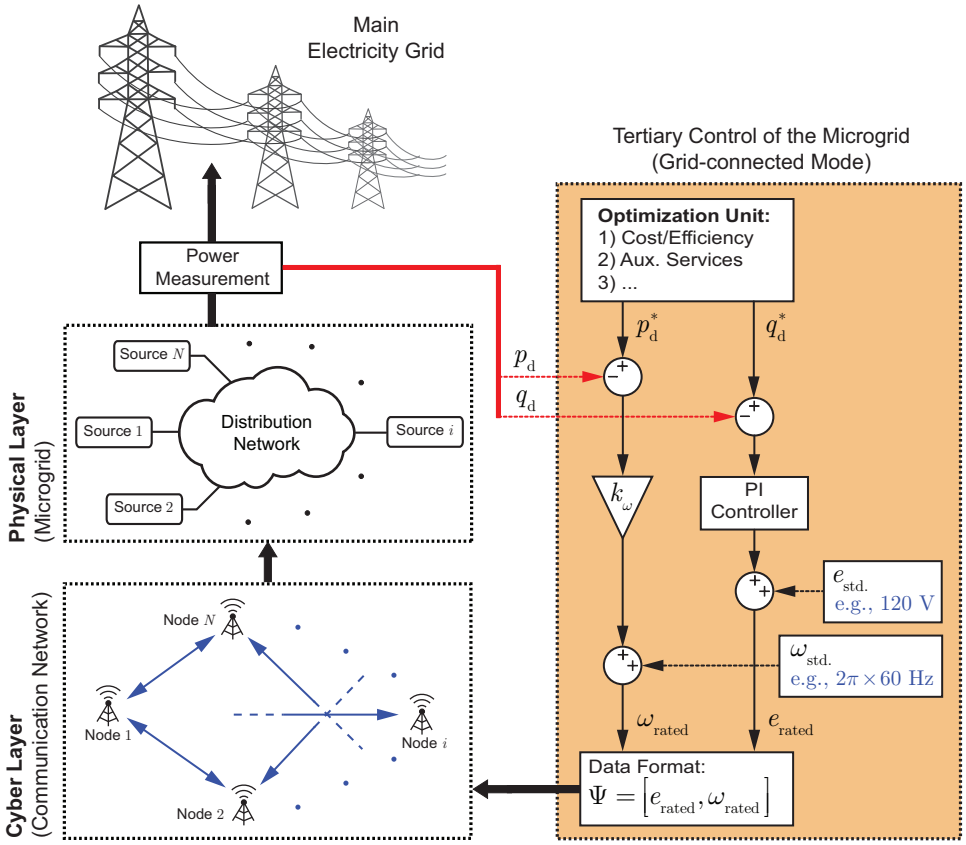

Fig. 4. Functionality of the tertiary controller in the grid-connected mode.

Functionality of the tertiary controller is elaborated in Fig. 4. The tertiary control unit runs cost/efficiency optimization to determine the desired active and reactive powers to be exchanges between the microgrid and the main grid, p_{d}^{*} and q_{d}^{*}, respectively. The optimization scenarios can also account for auxiliary services such as frequency regulation or reactive power support. It is noteworthy that the power flow between the microgrid and the main grid can be bidirectional and, thus, the desired powers p_{d}^{*} and q_{d}^{*} can be either positive or negative. The controller compares the actual powers supplied to the main grid, p_{d} and q_{d}, with the desired values and, accordingly, updates voltage and frequency ratings sent to the secondary controllers. The steady-state rated voltage assignment, e_{rated}, may have slight deviation from the standard value, however, the steady-state value of the rated frequency, ω_{rated}, will always converge to the standard value (e.g., 60 Hz in the North America). In fact, it is the transient variations in the rated frequency that adjusts the phase angles across the microgrid and manages the active power flow.

C. Voltage Estimation Policy

Each node has an estimation module that develops the estimation of the averaged voltage magnitude across the microgrid, e.g., $\overline{e}_i$, for Node i, and exchanges this estimation with its neighbors. The voltage estimation policy is demonstrated in Fig. 5.

Accordingly, the estimator at Node i updates its own output, $\overline{e}_i$, by processing the neighbors' estimates, $\overline{e}_j$ s ($j \in N_i$), and the local voltage measurement, e_i,

$$\overline{e}_i(t) = e_i(t) + \int_0^t \sum_{j \in N_i} a_{ij} \left(\overline{e}_j(\tau) - \overline{e}_i(\tau) \right) \mathrm{d}\tau. \tag{8}$$

This updating policy is commonly referred to as the *dynamic consensus protocol* in the literature [66]. As seen in (8), the local measurement, e.g., e_i, is directly fed into the estimation protocol. Thus, in case of any voltage variation at Node i, the local estimate, $\overline{e}_i$, immediately responds. The change in $\overline{e}_i$ propagates through the communication network and affects all other estimations. Assume that $\mathbf{e} = [e_1, e_2, \ldots, e_N]^{\mathrm{T}}$ and $\overline{\mathbf{e}} = [\overline{e}_1, \overline{e}_2, \ldots, \overline{e}_N]^{\mathrm{T}}$ are the measured voltage and the estimated average voltage vectors, respectively. $\mathbf{E}$ and $\overline{\mathbf{E}}$ are the Laplace transforms of $\mathbf{e}$ and $\overline{\mathbf{e}}$, respectively. Accordingly, global dynamic response of the estimation policy is formulated in [53] as

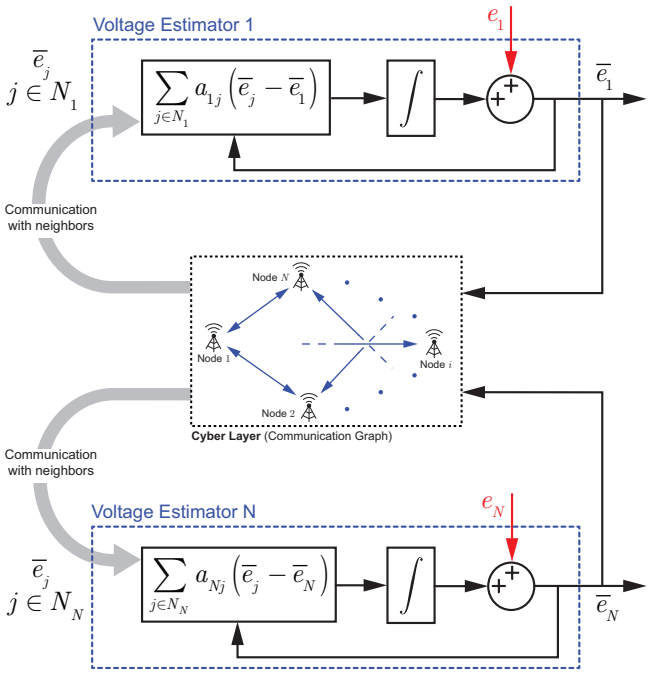

Fig. 5. Voltage averaging policy at each node; dynamic consensus protocol.

$$\overline{\mathbf{E}} = s(s\mathbf{I}_N + \mathbf{L})^{-1}\mathbf{E} = \mathbf{H}_{\mathrm{cst}}\mathbf{E}, \tag{9}$$

where $\mathbf{I}_N \in \mathbb{R}^{N \times N}$, $\mathbf{L}$, and $\mathbf{H}_{\mathrm{cst}}$ are the identity, Laplacian, and the estimator transfer-function matrices, respectively. It is shown in [53] that if the communication graph has a spanning tree with a balanced Laplacian matrix, $\mathbf{L}$, then, all elements of $\overline{\mathbf{e}}$ converge to a consensus value, which is the true average voltage, i.e., the average of all elements in $\mathbf{e}$. Equivalently,

$$\overline{\mathbf{e}}^{\mathrm{ss}} = \mathbf{M}\mathbf{e}^{\mathrm{ss}} = \left\langle \mathbf{e}^{\mathrm{ss}} \right\rangle \underline{\mathbf{1}}, \tag{10}$$

where $\mathbf{M} \in \mathbb{R}^{N \times N}$ is the averaging matrix, whose elements are all $1/N$. $\mathbf{x}^{\mathrm{ss}}$ expresses the steady-state value of the vector $\mathbf{x} \in \mathbb{R}^{N \times 1}$. $\langle \mathbf{x} \rangle$ is a scalar that represents the average of all elements in the vector $\mathbf{x}$. $\underline{\mathbf{1}} \in \mathbb{R}^{N \times 1}$ is a column vector whose elements are all one.

III. System-Level Modeling

System-level modeling studies the dynamic/static response of the entire microgrid with the proposed controller in effect. The system under study encompasses interactive cyber and physical subsystems. The communication graph topology defies the

interaction among controllers, functionality of the controllers determines output characteristics of the sources, and, finally, the transmission/distribution network rules the physical interaction among sources (and loads). Thus, the system-level study involves in mathematical modeling of each of the subsystems and establishment of mathematical coupling between the interactive subsystems.

A. Distribution Network Model

Dispatchable sources, transmission network, and loads form the physical layer of the microgrid. This layer is shown in Fig. 1(a), where sources are considered as controllable voltage source inverters. The proposed controller determines the voltage set pints (both magnitude, e_i^*, and phase, δ_i^*) for each source (i.e., inverter) by processing the supplied active and reactive powers. Such controller acts on the physical layer, which is a multi-input/multi-output plant with the voltage set points as the inputs and the supplied active and reactive powers as the outputs. Herein, we express the output variables, i.e., the supplied powers, in terms of the input variables, i.e., the voltage set points.

Figure 1(a) helps to formulate the supplied current of each source. By formulating the supplied current by Source i,

$$I_i = Y_{ii}V_i + \sum_{j=1(\neq i)}^{N} Y_{ij}(V_i - V_j), \tag{11}$$

where I_i and V_i are the phasor representation of the supplied current and phase voltage of the Source i, respectively. Y_{ii} and Y_{ij} are the local load admittance at Bus i (Source i) and the admittance of the transmission line connecting busses i and j, respectively. With no loss of generality, the distribution network is assumed reduced (i.e., by using Kron reduction) such that all non-generating busses are removed from the network. Thus, the complex power delivered by the Source i is,

$$s_i = 3V_iI_i^* = 3\left|V_i\right|^2 \sum_{j=1}^{N} Y_{ij}^* - 3\sum_{j=1(\neq i)}^{N} V_iV_j^*Y_{ij}^*. \tag{12}$$

Assume $V_i = e_i\angle\delta_i$ and $Y_{ij} = y_{ij}\angle\theta_{ij}$ where e_i, y_{ij}, δ_i, and θ_{ij} are the magnitude of V_i, magnitude of Y_{ij}, phase of V_i, and phase of Y_{ij}, respectively. $Y_{ij} = g_{ij} + jb_{ij}$ is the rectangular representation of the admittance Y_{ij}. One can use (12) to derive the active and reactive powers delivered by the Source i (p_i and q_i, respectively),

$$p_i = 3e_i^2\sum_{j=1}^{N} g_{ij} - 3\sum_{j=1(\neq i)}^{N} e_ie_jy_{ij}\cos(\delta_i - \delta_j - \theta_{ij}), \tag{13}$$

$$q_i = -3e_i^2\sum_{j=1}^{N} b_{ij} - 3\sum_{j=1(\neq i)}^{N} e_ie_jy_{ij}\sin(\delta_i - \delta_j - \theta_{ij}), \tag{14}$$

The secondary control typically acts slower than the dynamic of the power network (microgrid), as its objectives are voltage and power regulation in the steady state. Accordingly, one can safely neglect the fast dynamic transient responses of the microgrid and use the phasor analysis in (13)–(14) to model the power flow. Equations (13)–(14) express nonlinear

relationships between the voltages and supplied powers. In time domain, any variable x can be represented as $x = x^{\mathrm{q}} + \hat{x}$ where x^{q} and $\hat{x}$ are the quiescent and small-signal perturbation parts, respectively. Thus, one can write,

$$p_i = p_i^{\mathrm{q}} + \hat{p}_i = p_i^{\mathrm{q}} + \sum_{j=1}^{N} \frac{\partial p_i}{\partial e_j} \hat{e}_j + \sum_{j=1}^{N} \frac{\partial p_i}{\partial \delta_j} \hat{\delta}_j \quad \Rightarrow \hat{p}_i = \sum_{j=1}^{N} k_{e,ij}^{p} \hat{e}_j + \sum_{j=1}^{N} k_{\delta,ij}^{p} \hat{\delta}_j \tag{15}$$

$$q_i = q_i^{\mathrm{q}} + \hat{q}_i = q_i^{\mathrm{q}} + \sum_{j=1}^{N} \frac{\partial q_i}{\partial e_j} \hat{e}_j + \sum_{j=1}^{N} \frac{\partial q_i}{\partial \delta_j} \hat{\delta}_j \quad \Rightarrow \hat{q}_i = \sum_{j=1}^{N} k_{e,ij}^{q} \hat{e}_j + \sum_{j=1}^{N} k_{\delta,ij}^{q} \hat{\delta}_j \tag{16}$$

where the coefficients in (15)–(16) are formulated,

$$k_{e,ii}^{p} = \frac{p_i^{\mathrm{q}}}{e_i^{\mathrm{q}}} + 3e_i^{\mathrm{q}} \sum_{j=1}^{N} g_{ij}, \tag{17}$$

$$k_{e,ij}^{p} = -3e_i^{\mathrm{q}} y_{ij} \cos(\delta_i^{\mathrm{q}} - \delta_j^{\mathrm{q}} - \theta_{ij}), \quad j \neq i \tag{18}$$

$$k_{\delta,ii}^{p} = 3 \sum_{j=1(\neq i)}^{N} e_i^{\mathrm{q}} e_j^{\mathrm{q}} y_{ij} \sin(\delta_i^{\mathrm{q}} - \delta_j^{\mathrm{q}} - \theta_{ij}) = -q_i^{\mathrm{q}} - 3e_i^{2} \sum_{j=1}^{N} b_{ij}, \tag{19}$$

$$k_{\delta,ij}^{p} = -3e_i^{\mathrm{q}} e_j^{\mathrm{q}} y_{ij} \sin(\delta_i^{\mathrm{q}} - \delta_j^{\mathrm{q}} - \theta_{ij}), \quad j \neq i \tag{20}$$

$$k_{e,ii}^{q} = \frac{q_i^{\mathrm{q}}}{e_i^{\mathrm{q}}} - 3e_i^{\mathrm{q}} \sum_{j=1}^{N} b_{ij}, \tag{21}$$

$$k_{e,ij}^{q} = -3e_i^{\mathrm{q}} y_{ij} \sin(\delta_i^{\mathrm{q}} - \delta_j^{\mathrm{q}} - \theta_{ij}), \quad j \neq i \tag{22}$$

$$k_{\delta,ii}^{q} = -3 \sum_{j=1(\neq i)}^{N} e_i^{\mathrm{q}} e_j^{\mathrm{q}} y_{ij} \cos(\delta_i^{\mathrm{q}} - \delta_j^{\mathrm{q}} - \theta_{ij}) = p_i^{\mathrm{q}} - 3e_i^{2} \sum_{j=1}^{N} g_{ij}, \tag{23}$$

$$k_{\delta,ij}^{q} = 3e_i^{\mathrm{q}} e_j^{\mathrm{q}} y_{ij} \cos(\delta_i^{\mathrm{q}} - \delta_j^{\mathrm{q}} - \theta_{ij}), \quad j \neq i. \tag{24}$$

Equations (15)–(24) explain how a disturbance in any of the voltage magnitudes, $\hat{e}_i$ s, or phases, $\hat{\delta}_i$ s, affects the power flow in the entire microgrid. These equations can be represented in the matrix format,

$$\hat{\mathbf{p}} = \mathbf{k}_e^{p} \hat{\mathbf{e}} + \mathbf{k}_\delta^{p} \hat{\boldsymbol{\delta}} \tag{25}$$

$$\hat{\mathbf{q}} = \mathbf{k}_e^{q} \hat{\mathbf{e}} + \mathbf{k}_\delta^{q} \hat{\boldsymbol{\delta}} \tag{26}$$

where $\hat{\mathbf{p}} = \left[\hat{p}_1, \hat{p}_2, ..., \hat{p}_N\right]^{\mathrm{T}}$, $\hat{\mathbf{q}} = \left[\hat{q}_1, \hat{q}_2, ..., \hat{q}_N\right]^{\mathrm{T}}$, $\hat{\mathbf{e}} = \left[\hat{e}_1, \hat{e}_2, ..., \hat{e}_N\right]^{\mathrm{T}}$, and $\hat{\boldsymbol{\delta}} = \left[\hat{\delta}_1, \hat{\delta}_2, ..., \hat{\delta}_N\right]^{\mathrm{T}}$ are column vectors carrying small-signal portions of the active powers, reactive powers, voltage magnitudes, and voltage phases, respectively. $\mathbf{k}_e^{p} = [k_{e,ij}^{p}]$, $\mathbf{k}_\delta^{p} = [k_{\delta,ij}^{p}]$, $\mathbf{k}_e^{q} = [k_{e,ij}^{q}]$, and $\mathbf{k}_\delta^{q} = [k_{\delta,ij}^{q}]$ are all matrices in $\mathbb{R}^{N \times N}$ that contain coefficients in (17)–(24). $\mathbf{k}_\delta^{p}$ and $\mathbf{k}_e^{q}$ are referred to here as the $p-\delta$ and $q-e$ transfer matrices, respectively.

B. Dynamic Model of the Control and Cyber Subsystems

The cyber domain is where the controllers exchange measurements, process information and, update the voltage set points. Interactions and functionality of the controllers are shown in Fig. 2. One can see how the voltage and reactive power regulators cooperate to adjust the voltage magnitude set points, e_i^{*}. In the frequency domain,

$$G_i(s)\left(E_{\mathrm{rated}} - \bar{E}_i\right) = \Delta E_i^{1}, \tag{27}$$

$$H_i(s)\left(\sum_{j \in N_i} ba_{ij}(Q_j^{\mathrm{norm}} - Q_i^{\mathrm{norm}})\right) = \Delta E_i^{2}, \tag{28}$$

$$E_{\mathrm{rated}} + \Delta E_i^{1} + \Delta E_i^{2} = E_i^{*}, \tag{29}$$

where E_{rated}, $\bar{E}_i$, ΔE_i^{1}, Q_i^{norm}, ΔE_i^{2}, and E_i^{*} are the Laplace transforms of e_{rated}, $\bar{e}_i$, Δe_i^{1}, q_i^{norm}, Δe_i^{2}, and e_i^{*}, respectively. Equations (27)–(29) can be represented in the matrix format,

$$\mathbf{G}\left(\mathbf{E}_{\text{rated}}-\bar{\mathbf{E}}\right)=\mathbf{G}\left(\mathbf{E}_{\text{rated}}-\mathbf{H}_{\text{est}}\mathbf{E}\right)=\boldsymbol{\Delta}\mathbf{E}^{1}, \tag{30}$$

$$-b\mathbf{H}\mathbf{L}\mathbf{Q}^{\text{norm}}=-b\mathbf{H}\mathbf{L}\mathbf{q}_{\text{rated}}^{-1}\mathbf{Q}=\boldsymbol{\Delta}\mathbf{E}^{2}, \tag{31}$$

$$\mathbf{E}_{\text{rated}}+\boldsymbol{\Delta}\mathbf{E}^{1}+\boldsymbol{\Delta}\mathbf{E}^{2}=\mathbf{E}^{*}, \tag{32}$$

where $\mathbf{G}=\text{diag}\{G_i\}$ and $\mathbf{H}=\text{diag}\{H_i\}$ are diagonal matrices containing voltage and reactive power controllers, respectively. $\mathbf{G}$ and $\mathbf{H}$ are referred to as the voltage-controller and Q-controller matrices, respectively. $\mathbf{q}_{\text{rated}}=\text{diag}\{q_i^{\text{rated}}\}$ is a diagonal matrix that carries the rated reactive powers of the sources. $\mathbf{E}_{\text{rated}}=E_{\text{rated}}\underline{\mathbf{1}}$, $\boldsymbol{\Delta}\mathbf{E}^{1}=\left[\Delta E_i^1,\Delta E_2^1,...,\Delta E_N^1\right]^{\text{T}}$, $\boldsymbol{\Delta}\mathbf{E}^{2}=\left[\Delta E_i^2,\Delta E_2^2,...,\Delta E_N^2\right]^{\text{T}}$, $\mathbf{E}^{*}=\left[E_1^*,E_2^*,...,E_N^*\right]^{\text{T}}$, and $\mathbf{Q}^{\text{norm}}=\left[Q_1^{\text{norm}},Q_2^{\text{norm}},...,Q_N^{\text{norm}}\right]^{\text{T}}$ are column vectors carrying control variables.

It is assumed that for $t<0$ all sources of the microgrid operate with identical voltage set points, i.e., for all $1\le i\le N$, $e_i^*=e_{\text{rated}}$ and $\omega_i^*=\omega_{\text{rated}}$ and, thus, $v_i(t)=e_{\text{rated}}\sin(\omega_{\text{rated}}t)$. Then, the proposed controller is activated at $t=0$. Thus, the quiescent value of any variable x, x^{q}, represents its steady-state value for $t<0$, i.e., before activating the controller, and the small-signal part, $\hat{x}$, captures the variable response to the controller activation for $t>0$. Therefore, one can safely write $\boldsymbol{\delta}\mathbf{e}^{1,\text{q}}=\left[\delta e_1^{1,\text{q}},\delta e_2^{1,\text{q}},...,\delta e_N^{1,\text{q}}\right]^{\text{T}}=\mathbf{0}$, $\boldsymbol{\delta}\mathbf{e}^{2,\text{q}}=\left[\delta e_1^{2,\text{q}},\delta e_2^{2,\text{q}},...,\delta e_N^{2,\text{q}}\right]^{\text{T}}=\mathbf{0}$, and $\mathbf{e}_{\text{rated}}^{\text{q}}=e_{\text{rated}}\underline{\mathbf{1}}$ and, accordingly, simplify (30)–(31),

$$\mathbf{G}\left(\hat{\mathbf{E}}_{\text{rated}}-\mathbf{H}_{\text{est}}\hat{\mathbf{E}}\right)=\boldsymbol{\Delta}\hat{\mathbf{E}}^{1}, \tag{33}$$

$$-b\mathbf{H}\mathbf{L}\mathbf{q}_{\text{rated}}^{-1}\left(\frac{\mathbf{q}^{\text{q}}}{s}+\hat{\mathbf{Q}}\right)=\boldsymbol{\Delta}\hat{\mathbf{E}}^{2}, \tag{34}$$

where $\mathbf{q}^{\text{q}}=\left[q_1^{\text{q}},q_2^{\text{q}},...,q_N^{\text{q}}\right]^{\text{T}}$ carries the reactive powers supplied by individual sources for $t<0$. Since the rated voltage does not change before and after activating the controller, $\hat{\mathbf{E}}_{\text{rated}}=\mathbf{0}$. The voltage set points dynamics can now be found by substituting (33)–(34) into (32),

$$\hat{\mathbf{E}}^{*}=-\mathbf{G}\mathbf{H}_{\text{est}}\hat{\mathbf{E}}-b\mathbf{H}\mathbf{L}\mathbf{q}_{\text{rated}}^{-1}\left(\frac{\mathbf{q}^{\text{q}}}{s}+\hat{\mathbf{Q}}\right). \tag{35}$$

As seen, (35) has two terms. The first term, $-\mathbf{G}\mathbf{H}_{\text{est}}\hat{\mathbf{E}}$, represents the controller effort to achieve the global voltage regulation, and, the second term, $-b\mathbf{H}\mathbf{L}\mathbf{Q}_{\text{rated}}^{-1}\left(\mathbf{q}^{\text{q}}/s+\hat{\mathbf{Q}}\right)$, explains how the controller balances reactive load sharing across the microgrid.

Active power regulators (see Fig. 2) adjust the active power flow by tuning the phase angles. The controller at each source, e.g., Source i, compares its normalized active power with those of its neighbors and, accordingly, updates the phase angle set point as in (7). Controller activation at $t=0$ implies that $\omega_i^*(t<0)=\omega_{\text{rated}}$ and, thus, $\delta_i^{\text{q}}=\delta_i^{\text{ss}}(t<0)=0$. Accordingly,

$$\hat{\delta}_i^{*}(t\ge 0)=\int_0^t\sum_{j\in N_i}ca_{ij}(p_j^{\text{norm}}-p_i^{\text{norm}})\,\text{d}\tau. \tag{36}$$

Equivalently, in the frequency domain,

$$\hat{\Delta}_i^{*}=\frac{1}{s}\left(\sum_{j\in N_i}ca_{ij}(P_j^{\text{norm}}-P_i^{\text{norm}})\right), \tag{37}$$

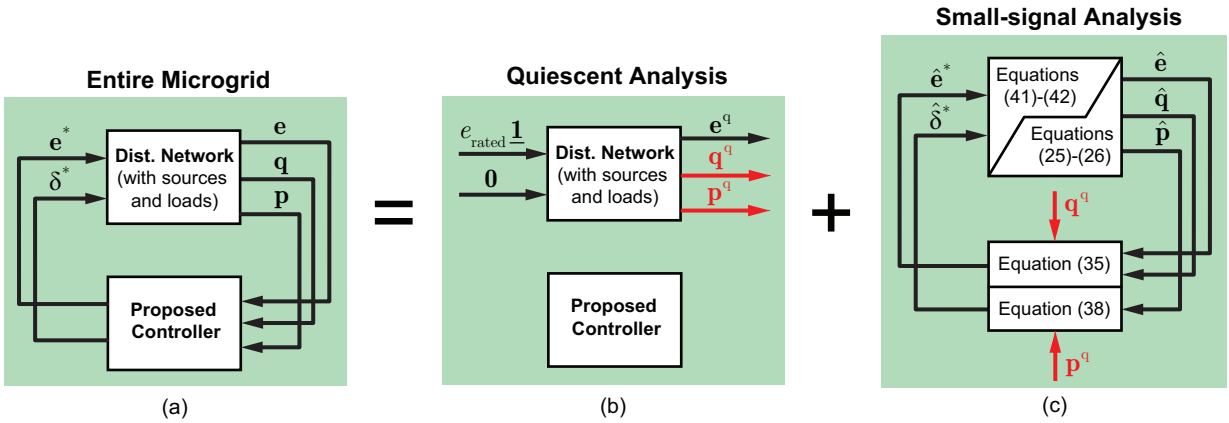

Fig. 6. Model of the entire microgrid: (a) Interaction between the physical layer and the control/cyber layer, (b) Quiescent analysis, (c) Small-signal analysis.

where $\hat{\Delta}_i^*$ is the Laplace transform of $\hat{\delta}_i^*$. One can write (37) in the matrix format,

$$\hat{\boldsymbol{\Delta}}^* = -\frac{c}{s}\mathbf{L}\mathbf{p}_{\text{rated}}^{-1}\mathbf{P} = -\frac{c}{s}\mathbf{L}\mathbf{p}_{\text{rated}}^{-1}\left(\frac{\mathbf{p}^{\text{q}}}{s}+\hat{\mathbf{P}}\right), \tag{38}$$

where $\hat{\boldsymbol{\Delta}}^* = \left[\hat{\Delta}_1^*, \hat{\Delta}_2^*, ..., \hat{\Delta}_N^*\right]^{\text{T}}$ and $\mathbf{p}_{\text{rated}} = \text{diag}\{p_i^{\text{rated}}\}$ is a diagonal matrix that includes the rated active powers of the sources. $\mathbf{p}^{\text{q}} = \left[\mathbf{p}_1^{\text{q}}, \mathbf{p}_2^{\text{q}}, ..., \mathbf{p}_N^{\text{q}}\right]^{\text{T}}$ carries the active powers supplied by individual sources before the controller activation, i.e., for $t<0$. Equation (38) represents the phase angles dynamic response to mitigate and, eventually, eliminate the active load sharing mismatch.

C. Dynamic Model of the Entire Microgrid

Figure 6 represents the model of the entire microgrid, which is separated into two sub-models; the quiescent model and the small-signal model. The entire system in the small-signal model can be treated as a multi-input/multi-output plant, where $\mathbf{p}^{\text{q}}/s$ and $\mathbf{q}^{\text{q}}/s$ are the inputs and $\hat{\mathbf{E}}$, $\hat{\mathbf{P}}$, and $\hat{\mathbf{Q}}$ are the outputs. Equations (35) and (38) show how the controller adjusts the voltage set points by processing the load sharing mismatches. Dynamic model of the inverters are studied in [67]–[69]. Accordingly, for the inverter driving the Source i, one can write,

$$\hat{\Delta}_i = G_i^{\Delta}\hat{\Delta}_i^*, \tag{39}$$

$$\hat{E}_i = G_i^{E}\hat{E}_i^*, \tag{40}$$

where G_i^E and G_i^{Δ} are the magnitude and phase transfer functions, respectively. Each inverter accommodates an output filter to eliminate the switching harmonics, whose dynamic is included in the transfer functions G_i^E and G_i^{Δ}. Equivalently, in the matrix format,

$$\hat{\boldsymbol{\Delta}} = \mathbf{G}^{\Delta}\hat{\boldsymbol{\Delta}}^*, \tag{41}$$

$$\hat{\mathbf{E}} = \mathbf{G}^{E}\hat{\mathbf{E}}^*, \tag{42}$$

where $\mathbf{G}^E = \text{diag}\{G_i^E\}$ and $\mathbf{G}^{\Delta} = \text{diag}\{G_i^{\Delta}\}$ are diagonal matrices of the inverter transfer functions. By substituting (35) and (38) in (25)–(26), and also using (41)–(42), one can formulate the entire system.

It is commonly assumed that the transmission/distribution network is predominantly inductive and, thus, active and reactive powers are mainly controlled by adjusting the voltage phases and magnitudes, respectively [70]. This assumption implies that in (25) and (26), $\mathbf{k}_e^p \simeq \mathbf{0}$ and $\mathbf{k}_\delta^q \simeq \mathbf{0}$, respectively, which helps to find the reduced-order dynamic model of the entire system. Substituting (41) in (38) and (42) in (35) yields

$$\left(\mathbf{G}^{\Delta}\right)^{-1}\hat{\boldsymbol{\Delta}} = -\frac{c}{s}\mathbf{L}\mathbf{p}_{\text{rated}}^{-1}\left(\frac{\mathbf{p}^{\text{q}}}{s}+\hat{\mathbf{P}}\right), \tag{43}$$

$$\left(\left(\mathbf{G}^{E}\right)^{-1}+\mathbf{G}\mathbf{H}_{\text{est}}\right)\hat{\mathbf{E}} = -b\mathbf{H}\mathbf{L}\mathbf{q}_{\text{rated}}^{-1}\left(\frac{\mathbf{q}^{\text{q}}}{s}+\hat{\mathbf{Q}}\right). \tag{44}$$

Substituting the reduced form of (25)–(26) in (43)–(44) yields

$$\hat{\mathbf{P}} = -\mathbf{T}_P\mathbf{L}\mathbf{p}_{\text{rated}}^{-1}\frac{\mathbf{p}^{\text{q}}}{s}, \tag{45}$$

$$\hat{\mathbf{Q}} = -\mathbf{T}_Q\mathbf{L}\mathbf{q}_{\text{rated}}^{-1}\frac{\mathbf{q}^{\text{q}}}{s}, \tag{46}$$

where, $\mathbf{T}_P$ and $\mathbf{T}_Q$ are the P–balancing and Q–balancing matrices, and are defied as,

$$\mathbf{T}_P \triangleq \left(s\left(c\mathbf{k}_\delta^p\mathbf{G}^{\Delta}\right)^{-1}+\mathbf{L}\mathbf{p}_{\text{rated}}^{-1}\right)^{-1}, \tag{47}$$

$$\mathbf{T}_Q \triangleq \left(\left(b\mathbf{k}_e^q\mathbf{G}^{E}\mathbf{H}\right)^{-1}+b^{-1}\mathbf{H}^{-1}\mathbf{G}\mathbf{H}_{\text{est}}\left(\mathbf{k}_e^q\right)^{-1}+\mathbf{L}\mathbf{q}_{\text{rated}}^{-1}\right)^{-1}. \tag{48}$$

Equations (43)–(48) describe dynamic response of the entire microgrid with the proposed controller in effect. Equations (45)–(46) describe that if the power (either active or reactive) was proportionally shared prior to activating the controller, i.e., $\mathbf{p}_{\text{rated}}^{-1}\mathbf{p}^{\text{q}} = n\underline{\mathbf{1}}$ or $\mathbf{q}_{\text{rated}}^{-1}\mathbf{q}^{\text{q}} = m\underline{\mathbf{1}}$, the power flow would remain intact after the controller activation, i.e., $\hat{\mathbf{p}}=\mathbf{0}$ or $\hat{\mathbf{q}}=\mathbf{0}$.

D. Controller Design Guideline

Appropriate selection of the control parameters is essential for proper operation of the proposed control methodology. For a given microgird, converter transfer function matrices, $\mathbf{G}^{\Delta}$ and $\mathbf{G}^{E}$, rated active and reactive matrices, $\mathbf{p}_{\text{rated}}$ and $\mathbf{q}_{\text{rated}}$, respectively, and $p-\delta$ and $q-e$ transfer matrices, $\mathbf{k}_\delta^p$ and $\mathbf{k}_e^q$, respectively, are known. Alternative communication networks may be chosen to exchange information; they, however, must satisfy three requirements; it should be a sparse graph with 1) at least a spanning tree, 2) balanced Laplacian matrix, and 3) minimum communication redundancy. Communication weights of the graph, a_{ij}, and, thus, the Laplacian matrix, $\mathbf{L}$, directly determine the voltage estimator dynamic, $\mathbf{H}_{\text{est}}$. One may tune the weights and examine the estimators dynamic through (9) to achieve a fast enough response. More details and insightful guidelines for optimal design of communication weights in cooperative systems can be found in [71].

Next, the designer may adjust the controller matrices $\mathbf{G}=\text{diag}\{G_i\}$ and $\mathbf{H}=\text{diag}\{H_i\}$ and the coupling gain b by evaluating (48) to place all poles of $\mathbf{T}_Q$ in the Open Left Hand Plane (OLHP). Intuitively, smaller gains help to stabilize the entire system while larger gains provide a faster dynamic response. Accordingly, the designer may decide the parameters by

making a trade-off between relative stability and settling time. The estimator dynamic should be considerably faster than the microgrid dynamics. Therefore, to evaluate (48), one can safely assume $\mathbf{H}_{\text{est}} \simeq \mathbf{M}$. Moreover, inverter switching frequency can be assumed high enough to provide a prompt response to the voltage command, i.e., $\mathbf{G}^{E} \simeq \mathbf{I}_{N}$.

As can be seen in Fig. 2, two separate modules, i.e., the voltage and the reactive power regulators, adjust the voltage magnitude, e_i^*, by generating two voltage correction terms, δe_i^1 and δe_i^2, respectively. As discussed in Section II-B, the voltage regulator is tasked to maintain average voltage across the microgrid at the rated value. Per such assignment, the voltage regulator must act fast to ensure voltage stability/regulation. On the other hand, the reactive power regulator is accountable for reactive load sharing in the steady state and its transient performance has less significance. Accordingly, the voltage control loops (including voltage estimators, controllers G_i s, and voltage measurement filters) must be designed for a higher bandwidth compared to the reactive power control loops (involving controllers H_i s and reactive power measurement filters). Typically, voltage measurement filters have a relatively high bandwidth as they only need to remove the switching harmonics. On the contrary, besides damping the switching harmonics, the active and reactive measurement units should filter out much lower frequency terms of the line-frequency harmonics and other contents caused by load nonlinearity or unbalance. Such design requirement slows down the power measurements process and, thus, the overall active/reactive load sharing control loops. Accordingly, as a design guideline, it is sufficient to choose the reactive power controllers H_i s to be slightly slower than the voltage controllers G_i s; low bandwidth power measurement filters automatically set the frequency response of the power regulators to be quite slower than the voltage regulator module.

Next step in the design procedure considers active power regulators. Equation (45) and (47) provide dynamic response of the active load sharing mechanism. Given the fast response of the inverters, one may assume $\mathbf{G}^{\Delta} \simeq \mathbf{I}_{N}$, which simplifies (47). The designer may sweep the coupling gain c and assess the stability and dynamic response through (47) to find an appropriate choice for c.

E. Steady-state Performance Analysis

The design guideline in Section III-D assures stable operation of the microgrid; physical variables such as voltages (magnitude and phase), system frequency, and supplied active and reactive powers would converge to steady-state values. This performance analysis investigates load sharing and voltage regulation quality in the steady state. To this end, assume that the system operates in the steady state for $t \geq t_0$. It should be noted that although the controller stabilizes voltages across the microgrid, one cannot simply deduce that the voltage and reactive power mismatches are zero. In other words, the inputs to the PI controllers G_i and H_i in Fig. 2 may be nonzero in the steady state, yet the two voltage correction terms δe_i^1 and δe_i^2

continuously vary with opposite rates such that sum of the two terms leaves a constant value and, thus, the voltage magnitude set point converges to a steady-state value. The following discussion attempts to show that such a scenario never happens; i.e., the mismatch inputs to both controllers decay to zero in the steady state, resulting in successful global voltage regulation and reactive load sharing. It also explains that the active power mismatch terms would all decay to zero, which provides the desired active load sharing while maintaining the rated frequency.

Voltage regulation and reactive load sharing is first to study. In the steady state, the voltage estimators converge to the true average voltage of the microgrid. Equivalently, $\overline{\mathbf{e}}^{\mathrm{ss}} = \mathbf{M}\mathbf{e}^{\mathrm{ss}} = \left\langle \mathbf{e}^{\mathrm{ss}} \right\rangle \underline{\mathbf{1}}$. Thus, based on the control methodology in Fig. 2, one can write

$$\begin{cases} \boldsymbol{\delta}\mathbf{e}^{1} = \boldsymbol{\delta}\mathbf{e}_{0}^{1} + \left(\mathbf{G}_{\mathrm{P}} + \mathbf{G}_{\mathrm{I}}(t-t_{0})\right)(e_{\mathrm{rated}}\underline{\mathbf{1}} - \mathbf{M}\mathbf{e}^{\mathrm{ss}}) \\ \boldsymbol{\delta}\mathbf{e}^{2} = \boldsymbol{\delta}\mathbf{e}_{0}^{2} + \left(\mathbf{H}_{\mathrm{P}} + \mathbf{H}_{\mathrm{I}}(t-t_{0})\right)(-b\mathbf{L}\mathbf{q}_{\mathrm{rated}}^{-1}\mathbf{q}^{\mathrm{ss}}) \end{cases}, \tag{49}$$

where $\boldsymbol{\delta}\mathbf{e}_{0}^{1}$ and $\boldsymbol{\delta}\mathbf{e}_{0}^{2}$ are column vectors that carry the integrator outputs in G_is and H_is at $t=t_0$, respectively. Accordingly,

$$\begin{aligned} \mathbf{e}^{*\mathrm{ss}} &= \mathbf{e}_{\mathrm{rated}} + \boldsymbol{\delta}\mathbf{e}^{1} + \boldsymbol{\delta}\mathbf{e}^{2} \\ &= e_{\mathrm{rated}}\underline{\mathbf{1}} + \boldsymbol{\delta}\mathbf{e}_{0}^{1} + \boldsymbol{\delta}\mathbf{e}_{0}^{2} + \mathbf{G}_{\mathrm{P}}(e_{\mathrm{rated}} - \left\langle \mathbf{e}^{\mathrm{ss}} \right\rangle)\underline{\mathbf{1}} - b\mathbf{H}_{\mathrm{P}}\mathbf{L}\mathbf{q}_{\mathrm{rated}}^{-1}\mathbf{q}^{\mathrm{ss}} \\ &\quad + \left(\mathbf{G}_{\mathrm{I}}(e_{\mathrm{rated}} - \left\langle \mathbf{e}^{\mathrm{ss}} \right\rangle)\underline{\mathbf{1}} - b\mathbf{H}_{\mathrm{I}}\mathbf{L}\mathbf{q}_{\mathrm{rated}}^{-1}\mathbf{q}^{\mathrm{ss}}\right)(t-t_{0}), \end{aligned} \tag{50}$$

where $\mathbf{G}_{\mathrm{I}}$ and $\mathbf{G}_{\mathrm{P}}$ are the diagonal matrices carrying the integral and proportional gains of the voltage-controller matrix $\mathbf{G}$ such that $\mathbf{G}_{\mathrm{P}} + \mathbf{G}_{\mathrm{I}}/s = \mathbf{G}$. Similarly, $\mathbf{H}_{\mathrm{I}}$ and $\mathbf{H}_{\mathrm{P}}$ are the diagonal matrices carrying the integral and proportional gains of the Q-controller matrix $\mathbf{H}$. Equation (50) holds for all $t \geq t_0$, and provides a constant voltage set point vector, $\mathbf{e}^{*\mathrm{ss}}$. Thus, the time-varying part of (50) is zero or, equivalently,

$$(e_{\mathrm{rated}} - \left\langle \mathbf{e}^{\mathrm{ss}} \right\rangle)\mathbf{U}\underline{\mathbf{1}} = \mathbf{L}\mathbf{q}_{\mathrm{rated}}^{-1}\mathbf{q}^{\mathrm{ss}}, \tag{51}$$

where $\mathbf{U} = b^{-1}\mathbf{G}_{\mathrm{I}}\mathbf{H}_{\mathrm{I}}^{-1} = \mathrm{diag}\{u_i\}$ is a diagonal matrix. Multiplying both sides of (51) from the left by $\underline{\mathbf{1}}^{\mathrm{T}}$,

$$(e_{\mathrm{rated}} - \left\langle \mathbf{e}^{\mathrm{ss}} \right\rangle)\underline{\mathbf{1}}^{\mathrm{T}}\mathbf{U}\underline{\mathbf{1}} = \underline{\mathbf{1}}^{\mathrm{T}}\mathbf{L}\mathbf{q}_{\mathrm{rated}}^{-1}\mathbf{q}^{\mathrm{ss}}. \tag{52}$$

Given the balanced Laplacian matrix, $\underline{\mathbf{1}}^{\mathrm{T}}\mathbf{L} = \mathbf{0}$ [54], which simplifies (52),

$$(e_{\mathrm{rated}} - \left\langle \mathbf{e}^{\mathrm{ss}} \right\rangle)\sum_{i=1}^{N} u_i = 0. \tag{53}$$

Since all entries of the matrix U are positive, (53) yields $e_{\mathrm{rated}} = \left\langle \mathbf{e}^{\mathrm{ss}} \right\rangle$, which implies that the controllers successfully regulates the averaged voltage magnitude of the microgrid, $\left\langle \mathbf{e}^{\mathrm{ss}} \right\rangle$, at the rated value, e_{rated}. Moreover, by substituting $e_{\mathrm{rated}} - \left\langle \mathbf{e}^{\mathrm{ss}} \right\rangle = 0$ in (51),

$$\mathbf{L}\mathbf{q}_{\mathrm{rated}}^{-1}\mathbf{q}^{\mathrm{ss}} = \mathbf{0}. \tag{54}$$

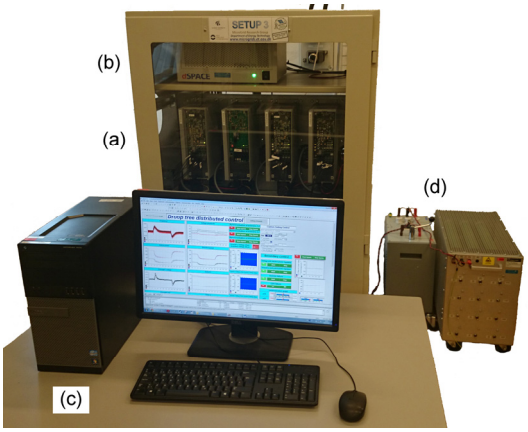

Fig. 7. AC microgrid prototype: (a) Inverter modules, (b) dSAPCE processor board (DS1006), (c) Programming and monitoring PC, (d) RL loads.

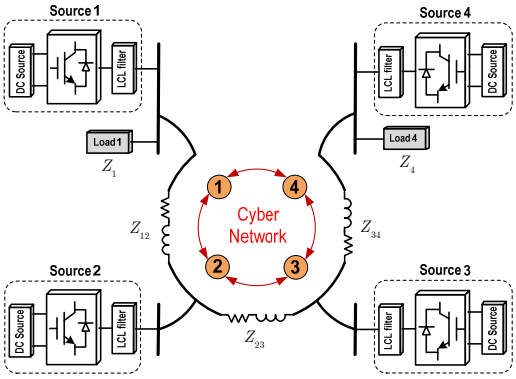

Fig. 8. Schematic of the microgrid prototype; radial electrical connection and ring cyber network.

If $\mathbf{L}$ is the Laplacian matrix associated with a graph that contains a spanning tree, the only nonzero solution to $\mathbf{Lx}=\mathbf{0}$ is $\mathbf{x}=n\underline{\mathbf{1}}$, where n is any real number [53]. Thus, (54) implies $\mathbf{q}^{\text{ss}}=n\mathbf{q}_{\text{rated}}\underline{\mathbf{1}}$, which assures that the controller shares the total reactive load among the sources in proportion to their ratings.

Frequency regulation and active load sharing is the next to study. The controller guarantees the convergence of the voltage magnitude vector, $\mathbf{e}$, and phase angle vector, $\boldsymbol{\delta}$ to steady-state values. Thus, (6)–(7) suggest that all sources would synchronize to the rated frequency, ω_{rated}. Moreover, based on (7), stabilizing the phase angles across the microgrid implies that all the frequency correction terms in (4) should decay to zero. Equivalently,

$$c\mathbf{L}\mathbf{p}_{\text{rated}}^{-1}\mathbf{p}^{\text{ss}}=\mathbf{0}, \tag{55}$$

which offers, $\mathbf{p}^{\text{ss}}=m\mathbf{p}_{\text{rated}}\underline{\mathbf{1}}$, where m is a positive real number. Thus, the controller successfully handles the proportional active load sharing.

IV. Experimental Validation

A $120/208$ V, 60 Hz three-phase AC microgrid, shown in Fig. 7, is prototyped in the Intelligent Microgrid Laboratory at Aalborg University. System schematic is described in Fig. 8, where four inverter-driven sources are placed in a radial connection to supply two loads, Z_1 and Z_4. The inverters (sources) have similar topologies but different ratings, i.e., the ratings of the inverters 1 and 2 are twice those for the inverters 3 and 4. Each inverter is augmented with an LCL filter to eliminate switching and line-frequency harmonics. RL-circuit model is used for each transmission line. An inductive-resistive distribution network is adopted to investigate collaborative interaction of the active and reactive power regulators in load sharing. Structure of the cyber network is highlighted in Fig. 8. Alternative cyber networks for a set of four agents in DC microgrids are discussed by authors in [53], [54] where the ring structure is shown to be the most effective option and, thus, is

considered here. It can be seen that the ring connection provides a sparse network that carries the required minimum redundancy, defined in Section II-A, where no single communication link failure would hinder the connectivity of the graph. Communication links are bidirectional to feature a balanced Laplacian matrix. A dSPACE processor board (DS1006) models the communication channels and implements the control routines. Electrical and control parameters of the microgrid are provided in the Appendix.

A. Performance Assessment

Figure 9 evaluates performance of the proposed control methodology. Inverters are initially driven with fixed voltage command, i.e., $e_i^* = 120\ \mathrm{V}$ and $\omega_i^* = 120\pi\ \mathrm{rad/s}$. It should be noted that no voltage feedback control had been initially in action to compensate the voltage drop across the LCL filters and, thus, the resulting bus voltages in Fig. 9(a) are less than the desired set point, i.e., $e_i^* = 120\ \mathrm{V}$. It can also be seen in Figs. 9(e) and 8(f) that the total load is not shared among sources in proportion to their power ratings.

It can be seen in the Appendix that the voltage controllers G_is are designed slightly faster than the reactive power controllers H_is. Cut-off frequencies of the power measurement filters are as low as $3\ \mathrm{Hz}$ to damp all undesired low-frequency harmonics. These design considerations set the dynamic responses of the two voltage and reactive power regulators apart enough to dynamically separate the two resulting voltage correction terms, i.e., δe_i^1 and δe_i^2. The proposed controller is activated at $t = 8\ \mathrm{s}$. The voltage correction terms have been added to the voltage set points to help with the global voltage regulation and reactive load sharing. Figure 9(a) demonstrates that the controllers have boosted the bus voltages across the microgrid to satisfy the global voltage regulation; i.e., for $t > 8\ \mathrm{s}$, the average voltage across the microgrid is successfully regulated at the desired $120\ \mathrm{V}$. As seen in Figs. 9(b) and 9(c), the first and the second voltage correction terms respond at two different time scales; the first correction term δe_i^1 (output of the voltage regulator) responds four times faster than the second correction term δe_i^2 (output of the reactive power regulator). Figure 9(b) shows that the controllers have varied the frequency set points in transients to adjust individual phase angles and provide the desired active load sharing. This figure supports the discussions in Section III-E, where the active power regulator is proven to only enforce transient deviations in frequency and that imposes no steady-state deviation. It can be seen that all inverter frequencies synchronize to the rated frequency of $60\ \mathrm{Hz}$ in the steady state. Figures 9(e) and 9(f) show the filtered power measurements and explain how the controllers have effectively rerouted the power flow to provide proportional load sharing. Individual and total reactive and active load demands are plotted in Figs. 9(g) and 9(h), respectively. It should be noted that the loads have drawn more power once the controller is activated since the voltages are boosted across the entire microgrid.

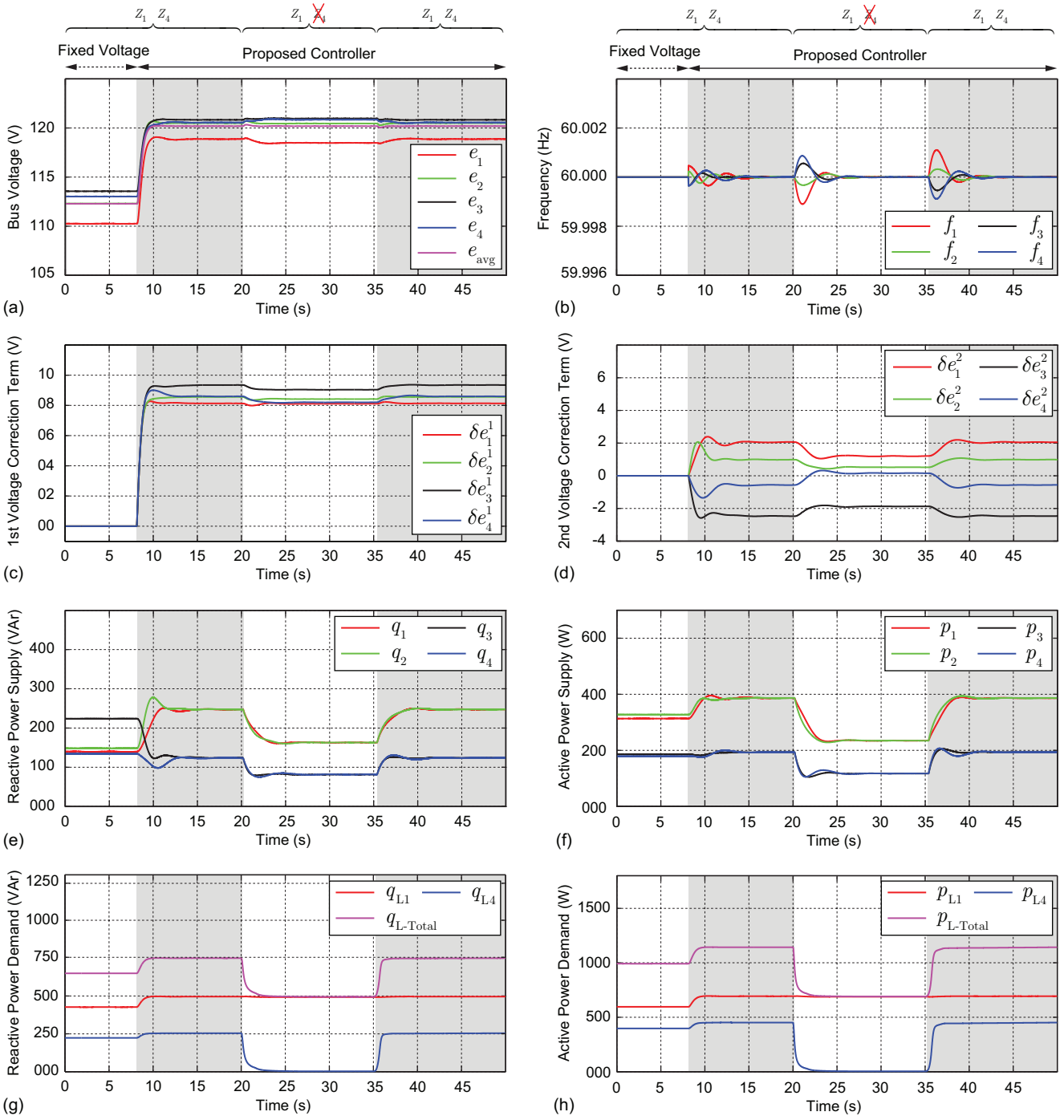

Fig. 9. Performance evaluation of the proposed controller: (a) Bus voltage (phase-to-neutral), (b) Inverter frequency set points, (c) First voltage correction term, δe_i^1, (d) Second voltage correction term, δe_i^2, (e) Supplied reactive power, (f) Supplied active power, (g) Load reactive power, and (h) Load active power. Power ratings of the inverters 1 and 2 are twice those of inverters 3 and 4.

Next, the controller performance is studied in response to the load change. The load at Bus 4, Z_4, has been unplugged at $t = 20$ s and plugged back in at $t = 35$ s. As seen in Fig. 9, the controller has successfully maintained global voltage regulation, frequency synchronization, and proportional load sharing, despite the change in load. It can also be observed in Figs. 9(e) and 9(f) that the inverters 3 and 4 respond faster to the load change than the other two inverters as they are in closer

vicinity of Z_4. Soft load change is performed in this study for safety purposes. In fact, the load inductor at Bus 4 features an air-gap control knob. Using this control opportunity, at $t = 20$ s, the load inductance is manually increased to its maximum value to provide an ultimate current damping feature. Then, the load is physically unplugged. A reverse procedure is followed at $t = 35$ s to plug the load, Z_4, back in. This soft load change procedure, besides the damping effect of the power measurement filters, explains why the supplied powers in Figs. 9(e) and 9(f) and the load demands in Figs. 9(g) and 9(h) show a slow and gradual profile rather than sudden changes.

B. Communication Delay and Channel Bandwidth

Communication is indispensable to access neighbor data and, thus, to the operation of distributed systems. Accordingly, channel non-idealities, e.g., transmission/propagation delay and limited bandwidth, and channel deficiencies such as packet loss may compromise the overall system performance. Thus, low delay and high bandwidth communication protocols are of paramount value for distributed control structures. For example, WiFi and Ultra Wide Band (UWB) protocols offer bandwidths up to 5 GHz and 7.5 GHz, respectively, with delays less than $1\ \mu$s. It should be noted that the length of the communication link directly affects the channel delay. Channel non-ideality effects on the controller performance has been studied in [72] for distributed systems and, particularly, for microgrids in [40], [73], and [74]. It is shown that such non-idealities have a negligible impact on the overall system performance if the channel delay is negligible compared to the controller dynamics. For the underlying microgrid, results in Fig. 9 clearly show that the controller dynamics are in the orders of hundreds of milliseconds (or longer); the system dynamics exhibit different time constants for the voltage, active, and reactive power regulation. Therefore, the proposed controller is expected to operate safely with most of the existing communication protocols. To further study the effect of communication delay and limited bandwidth, a detailed model of the underlying microgrid is simulated in MATLAB/SIMULINK environment. Figure 10 shows the transient load sharing performance in response to the step load change for a variety of communication delays and bandwidths. It should be noted that the results in this figure present *instantaneous* active and reactive powers; not the filtered measurements. However, the controller still processes the filtered quantities. Comparison of studies in Fig. 10 shows how large delays can compromise system stability (see Fig. 10(c)).

Analysis of distributed control protocols in [75] demonstrates that large communication delays impose dc errors on the voltage estimations and cause drift from a consensus. One can see such effect in Fig. 10, where longer delays introduce larger errors in voltage estimations and lead to bus voltages regulated at higher values than the desired rated voltage. This undesired voltage increment explains elevated supplied powers in Figs. 10(b) and 10(c) in comparison to Fig. 10(a).

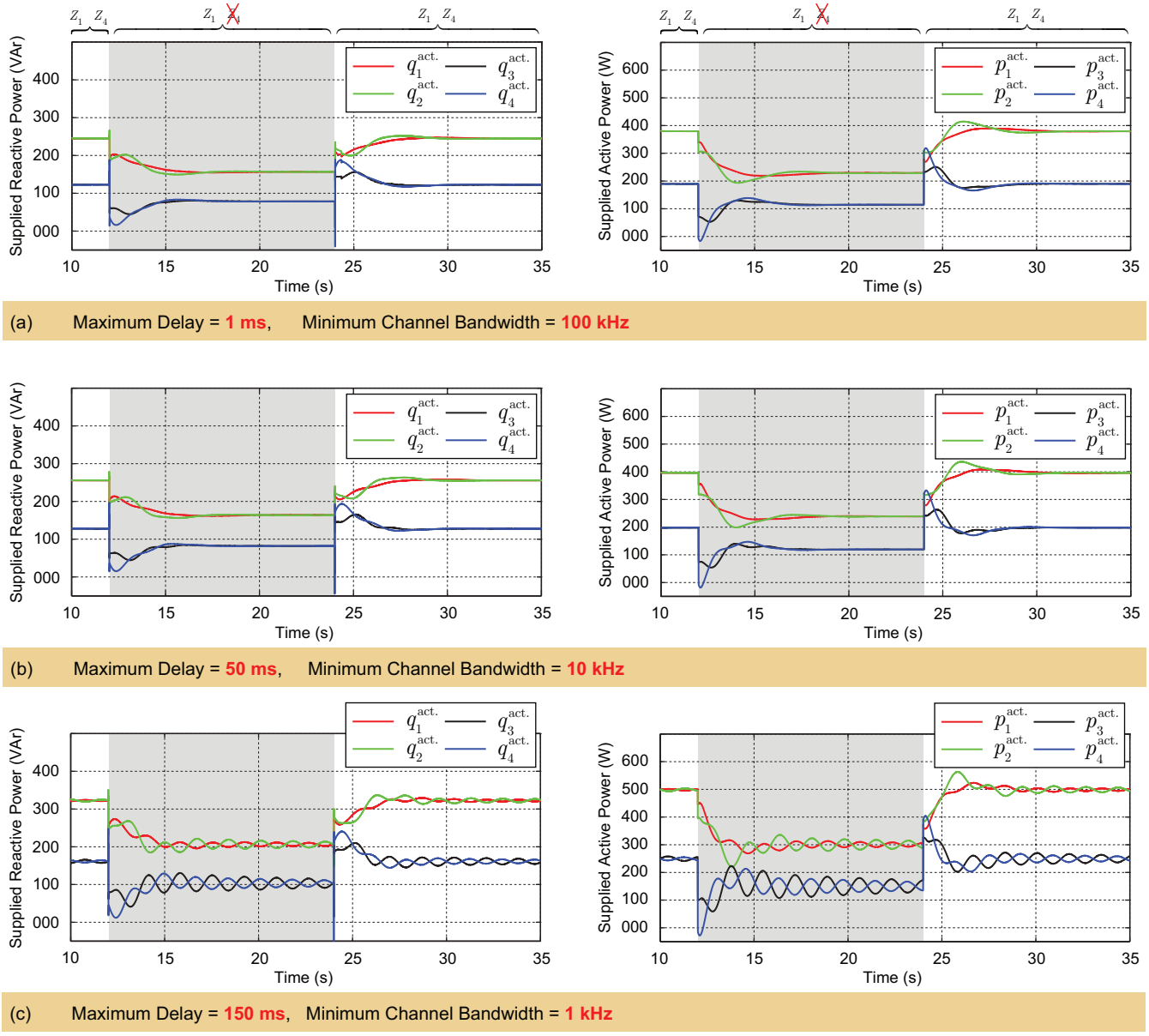

Fig. 10. Controller performance with non-ideal communication channel. Supplied active and reactive powers for (a) $\text{delay} = 1$ ms and $\text{BW} = 100$ kHz, (b) $\text{delay} = 50$ ms and $\text{BW} = 10$ kHz, and (c) $\text{delay} = 150$ ms and $\text{BW} = 1$ kHz.

Simulation studies ensure immunity of the controller performance to delays as long as 10 ms and channel bandwidths as low as 100 kHz, which makes communication protocols such as WiFi and UWB very suitable for the field implementation.

C. Plug-and-play Study

Figure 11 studies the plug-and-play capability of the proposed method. Inverter 3 has intentionally been unplugged at $t = 10$ s. Although this inverter is turned off instantly, the power measurements exponential decay to zero because of the existing low-pass filters.

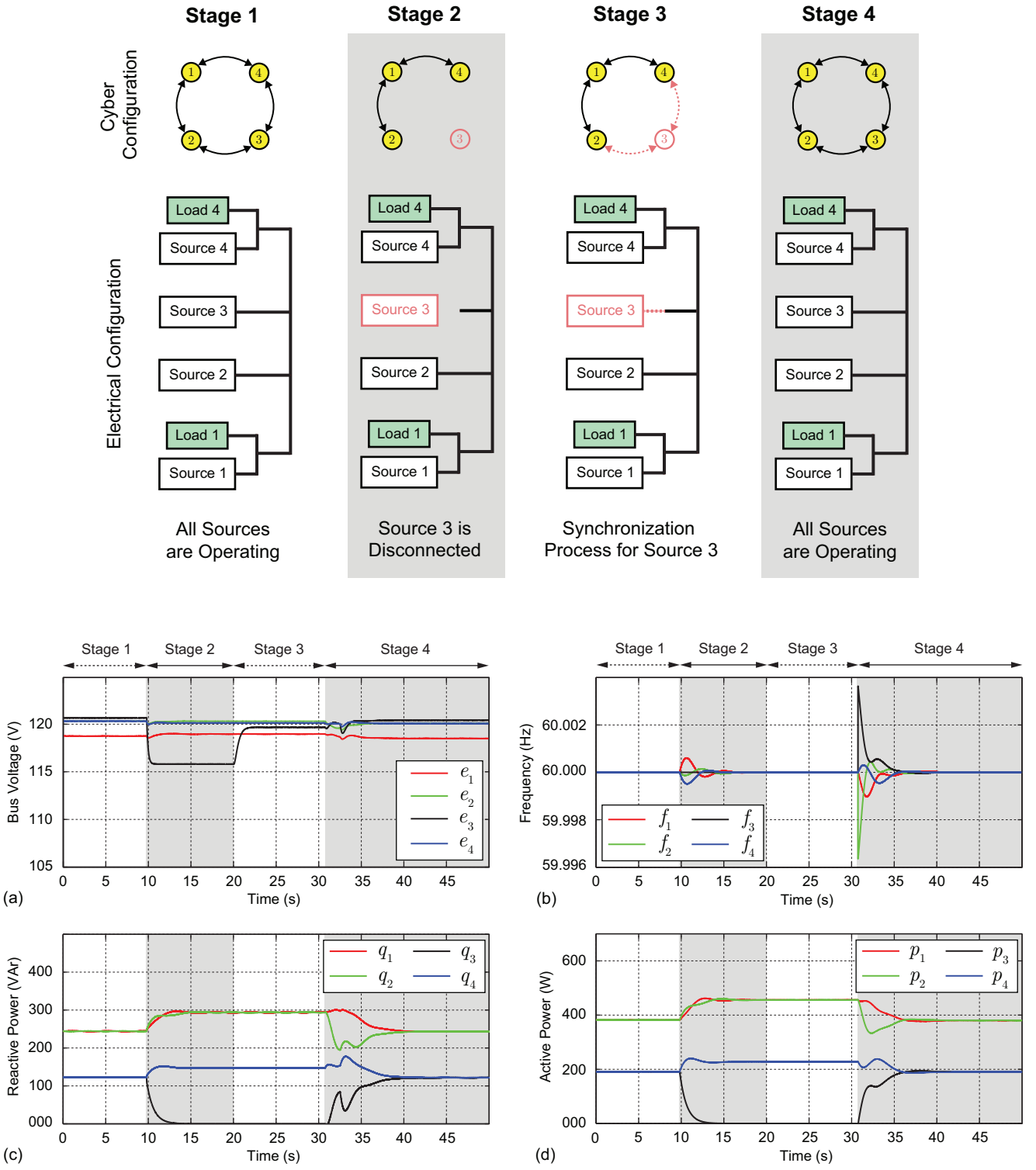

Fig. 11. Plug-and-play study for Inverter 3: (a) Bus voltage (phase-to-neutral), (b) Inverter frequency, (c) Supplied reactive power, and (d) Supplied active power.

It should be noted that a source failure also implies loss of all communication links connected to that particular source. Accordingly, when Source 3 fails, it automatically renders the links 2-3 (between Nodes 2 and 3) and 3-4 inoperable. However, as seen in Fig. 11, the remaining links still form a connected graph with balanced Laplacian matrix and, thus, the

control methodology should remain functional. As seen in Figs. 11(c) and 11(d), the controllers have successfully responded to the inverter loss and shared the excess power among the remaining inverters in proportion to their power ratings. After the loss of Inverter 3, the voltage measurement for Bus 3 would be unavailable. Thus, the controllers collectively regulate the new average voltage, i.e., the average voltage of the remaining three inverters, at the rated value of $120\ \mathrm{V}$. However, the actual average voltage across the microgrid is seen to be slightly less than the rated voltage. As seen in Fig. 11(a), Bus 3 experiences voltage sag due to the loss of generation. It should be noted that although inverter 3 is disconnected from Bus 3 the bus voltage is still available. Inverter 3 is plugged back in at $t = 20\ \mathrm{s}$; however, the synchronization procedure delays inverter engagement. After successful synchronization, the controller is activated at $t = 31\ \mathrm{s}$ and has shown excellent performance in the global voltage regulation and readjusting the load sharing to account for the latest plugged-in inverter.

D. Failure Resiliency in Cyber Domain

Resiliency to a single link failure is studied in Fig. 12. The original communication graph is designed to carry a minimum redundancy, such that no single communication link failure can compromise the connectivity of the cyber network. As seen in Fig. 12, the Link 3-4 has been disabled at $t = 3\ \mathrm{s}$, yet, it does not have any impact on the voltage regulation or load sharing, as the new graph is still connected and has a balanced Laplacian matrix. It should be noted that, by practicing error detection/control protocols in the communication modules, any link failure can be immediately detected at the receiving end. Accordingly, the receiving-end controller updates its set of neighbors by ruling out the node on the transmitting end of the failed link. This reconfiguration ensures that the misleading zero-valued data associated to the failed link (e.g., zero active and reactive power measurements) will not be processed by the receiving-end controller and, thus, the system remains functional.

The controller response to load change is then studied in Fig. 12 with the failed link, where a satisfactory performance is reported. In this study, the load at Bus 4, i.e., Z_4, has been unplugged and plugged back in at $t = 5\ \mathrm{s}$ and $t = 17.5\ \mathrm{s}$, respectively. It should be noted that although the link failure does not affect the steady-state performance, it slows down the system dynamics as it limits the information flow.

It should be noted that any reconfiguration in the cyber domain, e.g., communication link failure, affects the Laplacian matrix and, thus, the whole system dynamic. However, it will not compromise the steady-state performance of the control methodology, so long as the cyber network remains connected and presents a balanced Laplacian matrix. Connectivity of the cyber network plays a key role in the functionality of the entire microgrid. Including redundant cyber links, as discussed in sections II-A and II-B, ensures network connectivity for the most probable contingencies.

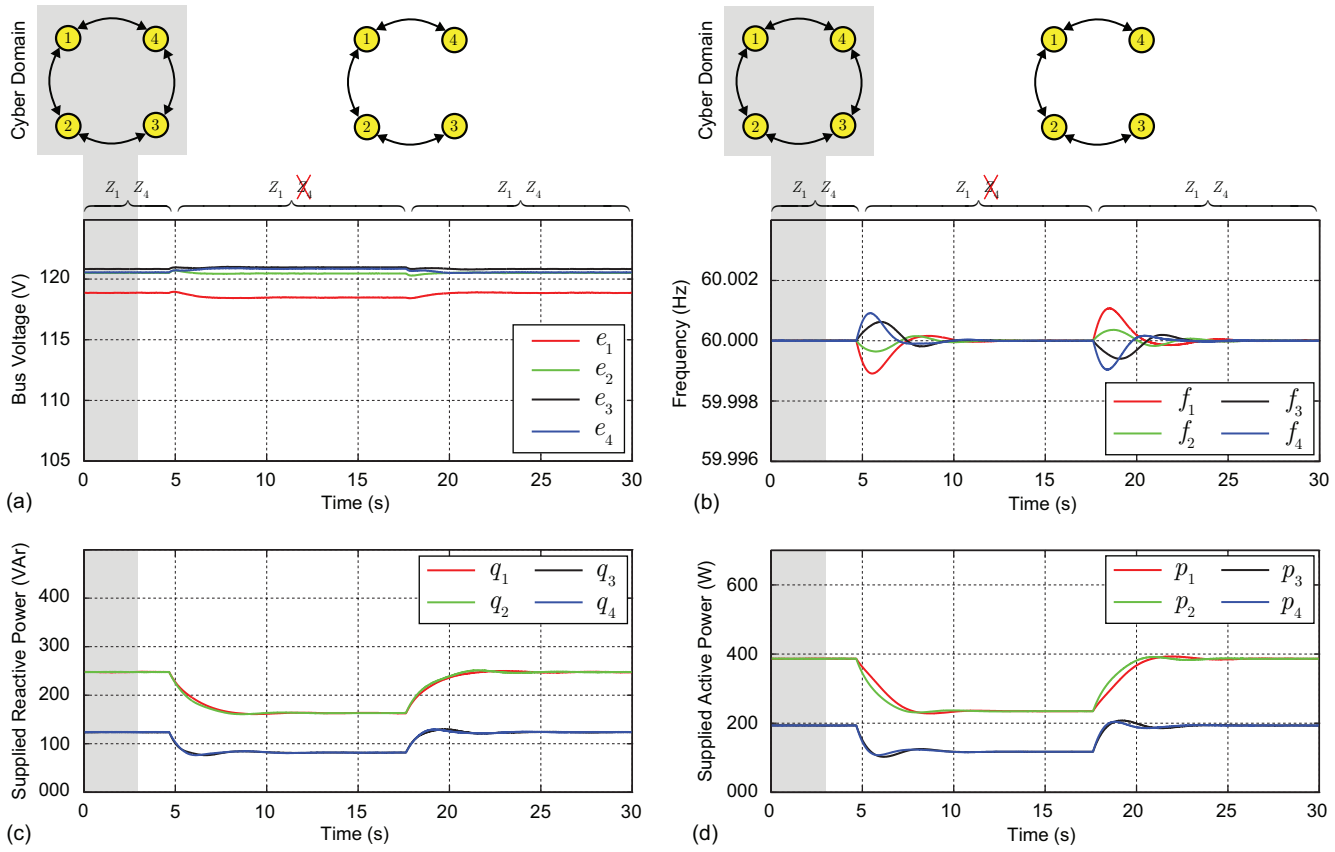

Fig. 12. Resiliency to failure in Link 3-4: (a) Bus voltage (phase-to-neutral), (b) Inverter frequency, (c) Supplied reactive power, and (d) Supplied active power.

However, any communication link failure requires immediate attention/maintenance before other links fail. It should be noted that it is very unlikely to lose connectivity due to simultaneous failures of several communication links.

V. Conclusion

A distributed secondary/primary controller is proposed for AC microgrids. The controller embedded on each inverter has three modules: the voltage, reactive power, and the active power regulators. The voltage regulator estimates the global average voltage across the microgrid. This estimation is then further used to adjust the local voltage set point. The reactive power regulator also adjusts the voltage set point by comparing the local normalized reactive power with the neighbors'. The active power regulator compares the local normalized active power with the neighbors' and, accordingly, adjusts the frequency (or, phase angle) set point to carry out the proportional active power sharing. This control paradigm does not rely on the droop mechanism, yet it is fully distributed, i.e., it uses a sparse communication network for data exchange among inverters. Experimental results show that the proposed cooperative control provides a precise global voltage regulation and proportional load sharing. Controller performance, plug-and-play capability, and resiliency to a single communication link failure are also verified through experiments.

APPENDIX

DC bus voltages that supply the inverter modules are all $V_{\rm dc} = 650\ \rm V$. The filter inductors are identical and $L_{\rm F1} = L_{\rm F2} = 1.8\ \rm mH$, and the intermediate capacitor is $C_{\rm F} = 25\ \mu\rm F$. The line impedance connecting busses i and j can be expressed as $Z_{ij} = R_{ij} + sL_{ij}$ where,

$$\begin{cases} R_{12} = 0.8\ \Omega & L_{12} = 3.6\ \rm mH \\ R_{23} = 0.4\ \Omega & L_{23} = 1.8\ \rm mH \\ R_{34} = 0.7\ \Omega & L_{34} = 1.5\ \rm mH \end{cases}. \tag{A.1}$$

The control parameters are,

$$\begin{cases} \mathbf{p}_{\rm rated} = 1\ \rm kW \times \rm diag\{1.6, 1.6, 0.8, 0.8\} \\ \mathbf{q}_{\rm rated} = 1\ \rm kVAr \times \rm diag\{0.6, 0.6, 0.3, 0.3\} \end{cases}, \tag{A.2}$$

$$\mathbf{A}_{\mathbf{G}} = 1.5 \times \begin{bmatrix} 0 & 1 & 0 & 1 \\ 1 & 0 & 1 & 0 \\ 0 & 1 & 0 & 1 \\ 1 & 0 & 1 & 0 \end{bmatrix}, \tag{A.3}$$

$$b = 2, \quad c = 0.02, \tag{A.4}$$

$$\begin{cases} \mathbf{G}_{\rm P} = 0.01 \times \mathbf{I}_4, & \mathbf{G}_{\rm I} = 3 \times \mathbf{I}_4 \\ \mathbf{H}_{\rm P} = 0.005 \times \mathbf{I}_4, & \mathbf{H}_{\rm I} = 2 \times \mathbf{I}_4 \end{cases}. \tag{A.5}$$

REFERENCES

[1] J. M. Guerrero, J. C. Vasquez, J. Matas, L. G. de Vincuña, and M. Castilla, "Hierarchical control of droop-controlled ac and dc microgrids – A general approach toward standardization," *IEEE Trans. Ind. Electron.*, vol. 58, pp. 158–172, Jan. 2011.

[2] R. Majumder, B. Chaudhuri, A. Ghosh, R. Majumder, G. Ledwich, and F. Zare, "Improvement of stability and load sharing in an autonomous Microgrid using supplementary droop control loop," *IEEE Trans. Power Syst.*, vol. 25, no. 2, pp. 796–808, May 2010.

[3] H. Kakigano, Y. Miura, and T. Ise, "Distribution voltage control for dc Microgrids using fuzzy control and gain-scheduling technique," *IEEE Trans. Power Electron.*, vol. 28, no. 5, pp. 2246–2258, May 2013.

[4] I. U. Nutkani, P. C. Loh, P. Wang, and F. Blaabjerg, "Cost-prioritized droop schemes for autonomous ac microgrids," *IEEE Trans. Power Electron.*, vol. 30, no. 2, pp. 1109–1119, Feb. 2015.

[5] P. C. Loh, D. Li; Y. K. Chai, and F. Blaabjerg, "Autonomous operation of hybrid microgrid with ac and dc subgrids," *IEEE Trans. Power Electron.*, vol. 28, no. 5, pp. 2214–2223, May 2013.

[6] M. Datta, T. Senjyu, A. Yona, T. Funabashi, and C. H. Kim, "A frequency-control approach by photovoltaic generator in a PV-diesel hybrid power system," *IEEE Trans. Energy Convers.*, vol. 26, no. 2, pp. 559–571, Jun. 2011.

[7] C. K. Sao and W. Lehn, "Control and power management of converter-fed microgrids," *IEEE Trans. Power Syst.,* vol. 23, pp. 1088–1098, Aug. 2008.

[8] E. Serban and H. Serban, "A control strategy for a distributed power generation microgrid application with voltage- and current-controlled source converter," *IEEE Trans. Power Electron.*, vol. 15, pp. 2981–2992, Dec. 2010.

[9] A. Bidram and A. Davoudi, "Hierarchical structure of microgrids control system," *IEEE Trans. Smart Grid*, vol. 3, pp. 1963–1976, Dec 2012.

[10] J. C. Vasquez, J. M. Guerrero, J. Miret, M. Castilla, and L.G. de Vicuña, "Hierarchical control of intelligent microgrids," *IEEE Ind. Electron. Mag.*, vol. 4, pp. 23–29, Dec. 2010.

[11] J. A. P. Lopes, C. L. Moreira, and A. G. Madureira, "Defining control strategies for microgrids islanded operation," *IEEE Trans. Power Syst.,* vol. 21, pp. 916–924, May 2006.

[12] F. Katiraei, M. R. Iravani, and P. W. Lehn, "Microgrid autonomous operation during and subsequent to islanding process," *IEEE Trans. Power Del.,* vol. 20, pp. 248–257, Jan. 2005.

[13] M. Savaghebi, A. Jalilian, J. Vasquez, and J. Guerrero, "Secondary control for voltage quality enhancement in microgrids," *IEEE Trans. Smart Grid,* vol. 3, pp. 1893–1902, Dec. 2012.

[14] H. Kanchev, D. Lu, F. Colas, V. Lazarov, and B. Francois, "Energy management and operational planning of a microgrid with a PV-based active generator for smart grid applications," *IEEE Trans. Ind. Electron.*, vol. 58, no. 10, pp. 4583–4592, Oct. 2011.

[15] C. Chen, S. Duan, T. Cai, B. Liu, and G. Hu, "Optimal allocation and economic analysis of energy storage system in microgrids," *IEEE Trans. Power Electron.*, vol. 26, no. 10, pp. 2762–2773, Oct. 2011.

[16] N. Ainsworth and S. Grijalva, "A structure-preserving model and sufficient condition of frequency synchronization of lossless droop inverter-based ac network," *IEEE Trans. Power Syst.*, vol. 28, pp. 4310–4319, Nov. 2013.

[17] D. Wu, F. Tang, J. M. Guerrero, and J. C. Vasquez, "Autonomous control of distributed generation and storage to coordinate P/Q sharing in islanded microgrids – An approach beyond droop control," in *Proc. IEEE Int. Energy Conf.*, 2014, pp. 983–988.

[18] J. Y. Kim, J. H. Jeon, S. K. Kim, C. Cho, J. H. Park, H. M. Kim, and K. Y. Nam, "Cooperative control strategy of energy storage system and micro sources for stabilizing the microgrid during islanded operation," *IEEE Trans. Power Electron.*, vol. 25, pp. 3037–3048, Dec. 2010.

[19] S. M. Ashabani and Y. A. R. I. Mohamed, "General interface for power management of micro-grids using nonlinear cooperative droop control," *IEEE Trans. Power Syst.*, vol. 28, pp. 2929–2941, Aug. 2013.

[20] J. Hu, J. Zhu, D. G. Dorrell, and J. M. Guerrero, "Virtual flux droop method – A new control strategy of inverters in microgrids," *IEEE Trans. Power Electron.*, vol. 29, pp. 4704–4711, Sept. 2014.

[21] Y. A. I. Mohamed and E. F. El-Saadany, "Adaptive decentralized droop controller to preserve power sharing stability of paralleled inveretrs in distributed generation microgrids," *IEEE Trans. Power Electronics*, vol. 23, pp. 2806–2816, Nov. 2008.

[22] J. He and Y. W. Li, "Analysis, design, and implementation of virtual impedance for power electronics interfaced distributed generation," *IEEE Trans. Ind. Appl.*, vol. 41, pp. 2525–2538, Nov./Dec. 2011.

[23] J. W. Simpson-Porco, F. Dorfler, and F. Bullo, "Voltage stabilization in microgrids via quadratic droop control," *IEEE 52nd Annu. Conf. Decision and Control*, 2013, pp. 7582–7589.

[24] H. Mahmood, D. Michaelson, and J. Jiang, "Accurate reactive power sharing in an islanded microgrid using adaptive virtual impedances," *IEEE Trans. Power Electron.*, vol. 30, no. 3, pp. 1605–1617, Mar. 2015.

[25] H. Han, Y. Liu, Y. Sun, M. Su, and J. M. Guerrero, "An improved droop control strategy for reactive power sharing in islanded microgrid," *IEEE Trans. Power Electron.*, vol. 30, no. 6, pp. 3133–3141, Jun. 2015.

[26] J. Rocabert, A. Luna, F. Blaabjerg, and P. Rodriguez, "Control of power converters in ac microgrids," *IEEE Trans. Power Electron.*, vol. 27, pp. 4734–4749, Nov. 2012.

[27] C. T. Lee, C. C. Chu, and P. T. Cheng, "A new droop control method for the autonomous operation for distribute energy resource interface converters," *IEEE Trans. Power Electron.*, vol. 28, pp. 1980–1993, Apr. 2013.

[28] S. V. Dhople. B. B. Johnson, and A. O. Hamadeh, "Virtual oscillator control for voltage source inverters," in *Proc. 51st Annu. Allerton Conf.*, 2013, pp. 1359–1363.

[29] B. B. Johnson, S. V. Dhople. A. O. Hamadeh, and P. T. Krein, "Synchronization of nonlinear oscillators in an LTI electrical power network," *IEEE Trans. Circuits Syst. I: Reg. Papers*, vol. 61, pp. 834–844, Mar. 2014.

[30] B. B. Johnson, S. V. Dhople. A. O. Hamadeh, and P. T. Krein, "Synchronization of parallel single-phase inverters with virtual oscillator control," *IEEE Trans. Power Electron.*, vol. 29, no. 11, pp. 6124–6138, Nov. 2014.

[31] B. B. Johnson, S. V. Dhople, J. L. Cale, A. O. Hamadeh, and P. T. Krein, "Oscillator-based inverter control for islanded three-phase microgrids," IEEE J. *Photovoltaics*, vol. 4, no. 1, pp. 387–395, Jan. 2014.

[32] T. L. Vandon, B. Meersman, J. D. M. De Koonig, and L. Vandevelde, "Analogy between conventional grid control and islanded microgrid control based on a global dc-link voltage droop," *IEEE Trans. Power Del.*, vol. 27, pp. 1405–1414, July 2012.

[33] A. H. Etemadi, E. J. Davison, R. Iravani, "A decentralized robust strategy for multi-DER microgrids – Part I: Fundamental concepts," *IEEE Trans. Power Del.*, vol. 27, pp. 1843–1853, Oct. 2012.

[34] Q. Shafiee, V. Nasirian, J. M. Guerrero, F. L. Lewis, and A. Davoudi, "Team-oriented adaptive droop control for autonomous AC microgrids," in *Proc. 40th Ind. Electron. Conf. (IECON)*, 2014, pp. 1861–1867.

[35] A. Micallef, M. Apap, C. Spiteri-Staines, J. M. Guerrero, and J. C. Vasquez, "Reactive power sharing and voltage harmonic distortion compensation of droop controlled single phase islanded microgrids," *IEEE Trans. Smart Grid*, vol. 5, pp. 1149–1158, May 2014.

[36] A. Mehrizi-Sani and R. Iravani, "Potential-function based control of a microgrid in islanded and grid-connected modes," *IEEE Trans. Power Syst.,* vol. 25, pp. 1883–1891, Nov. 2010.

[37] A. Mehrizi-sani and R. Iravani, "Constrained potential function-based control of microgrids for improved dynamic performance," *IEEE Trans. Smart Grid*, vol. 3, pp. 1885–1892, Dec. 2012.

[38] A. H. Etemadi, E. J. Davison, R. Iravani, "A decentralized robust strategy for multi-DER microgrids – Part II: Performance evaluation," *IEEE Trans. Power Del.*, vol. 27, pp. 1854–1861, Oct. 2012.

[39] A. H. Etemadi, E. J. Davison, R. Iravani, "A generalized decentralized robust control of islanded microgrids," *IEEE Trans. Power Syst.*, vol. 29, no. 6, pp. 3102–3113, Nov. 2014.

[40] A. Kahrobaeian and Y. A. R. I. Mohamed, "Networked-based hybrid distributed power sharing and control of islanded micro-grid systems," *IEEE Trans. Power Electron.*, vol. 30, no. 2, pp. 603–617, Feb. 2015.

[41] Q. Hui and W. Haddad, "Distributed nonlinear control algorithms for network consensus," *Automatica*, vol. 42, pp. 2375–2381, Sept. 2008.

[42] J. Fax and R. Murray, "Information flow and cooperative control of vehicle formations," *IEEE Trans. Automat. Control*, vol. 49, pp. 1465–1476, Sept. 2004.

[43] Z. Qu, *Cooperative control of dynamical systems: Applications to autonomous vehicles*. New York: Springer-Verlag, 2009.

[44] Q. Shafiee, J. M. Guerrero, and J. C. Vasquez, "Distributed secondary control for islanded microgrids – A novel approach," *IEEE Trans. Power Electron.*, vol. 29, pp. 1018–1031, Feb. 2014.

[45] Q. Shafiee, C. Stefanovic, T. Dragicevic, P. Popovski, J. C. Vasquez, and J. M. Guerrero, "Robust networked control scheme for distributed secondary control of islanded microgrids," *IEEE Trans. Ind. Electron.*, vol. 61, pp. 5363–5374, Oct. 2014.

[46] Y. Zhang and H. Ma, "Theoretical and experimental investigation of networked control for parallel operation of inverters," *IEEE Trans. Ind. Electron.*, vol. 59, pp. 1961–1970, Apr. 2012.

[47] M. N. Marwali and A. Keyhani, "Control of distributed generation systems – Part I: Voltages and currents control," *IEEE Trans. Power Electron.*, vol. 19, pp. 1541–1550, Nov. 2004.

[48] M. N. Marwali, J. W. Jung, and A. Keyhani, "Stability analysis of load sharing control for distributed generation systems," *IEEE Trans. Energy Convers.*, vol. 22, pp. 737–745, Sept. 2004.

[49] S. D. J. McArthur, E. M. Davidson, V. M. Catterson, A. L. Dimeas, N. D. Hatziargyriou, F. Ponci, and T. Funabashi, "Multi-agent systems for power engineering applications – part I: Concepts, approaches, and technical challenges," *IEEE Trans. Power Syst.,* vol. 22, pp. 1743–1752, Nov. 2007.

[50] A. Bidram, A. Davoudi, and F. L. Lewis, "A multi-objective distributed control framework for islanded microgrids," *IEEE Trans. Ind. Informatics*, vol. 10, no. 3, pp. 1785–1798, Aug. 2014.

[51] A. Bidram, A. Davoudi, F. L. Lewis, and Z. Qu, "Secondary control of microgrids based on distributed cooperative control of multi-agent systems," *IET Generation, Transmission Dist.*, vol. 7, pp. 822–831, Aug. 2013.

[52] V. Nasirian, A. Davoudi, and F. L. Lewis, "Distributed adaptive droop control for dc microgrids," in *Proc. 29th IEEE Appl. Power Electron. Conf. Expo. (APEC)*, 2014, pp. 1147–1152.

[53] V. Nasirian, S. Moayedi, A. Davoudi, and F. L. Lewis, "Distributed cooperative control of dc microgrids," *IEEE Trans. Power Electron.*, vol. 30, pp. 2288–2303, Apr. 2015.

[54] V. Nasirian, A. Davoudi, F. L. Lewis, and J. M. Guerrero, "Distributed adaptive droop control for dc distribution systems," *IEEE Trans. Energy Convers.*, vol. 29, pp. 944–956, Dec. 2014.

[55] S. Moayedi, V. Nasirian, F. L. Lewis, and A. Davoudi, "Team-oriented load sharing in parallel dc-dc converters," *IEEE Trans. Ind. Appl.*, vol. 51, no. 1, pp. 479–490, Jan./Feb. 2015.

[56] B. A. Robbins, C. N. Hadjicostis, and A. D. Dominguez-Garcia, "A two-stage distributed architecture for voltage control in power distribution systems," *IEEE Trans. Power Syst.*, vol. 28, pp. 1470–1482, May 2013.
[57] A. D. Dominguez-Garcia, C. N. Hadjicostis, and N. F. Vaidya, "Resilient networked control of distributed energy resources," *IEEE J. Sel. Areas Commun.*, vol. 30, pp. 113–1148, Jul. 2012.
[58] S. T. Cady and A. D. Dominguez-Garcia, "Distributed generation control of small-footprint power systems," in *Proc. North American Power Symp.*, 2012, pp. 1–6.
[59] F. Dorfler,J. W. Simpson-Porco, and F. Bullo, "Breaking the hierarchy: Distributed control and economic optimality in microgrids," 2014, Available on arXiv:1401.1767v1.
[60] H. Bouattour, J. W. Simpson-Porco, F. Dorfler, and F. Bullo, "Further results on distribute secondary control in microgrids," *IEEE Conf. on Decision and Control*, 2013, pp.1514–1519.
[61] J. W. Simpson-Porco, F. Dorfler, F. Bullo, Q. Shafiee, and J. M. Guerrero, "Stability, power sharing, and distributed secondary control in droop-controlled microgrids," *IEEE Smart Grid Commun. Symp.*, 2013, pp. 672–677.
[62] J. W. Simpson-Porco, F. Dorfler, and F. Bullo, "Synchronization and power sharing for droop-controlled inverters in islanded microgrids," *Automatica*, vol. 49, pp. 2603–2611, Jun. 2013.
[63] R. Olfati-saber, J. A. Fax, and R. M. Murray, "Consensus and cooperation in networked multi-agent systems," *Proc. IEEE*, vol. 95, no. 1, pp. 215–233, Jan. 2007.
[64] R. Olfati-Saber and R. M. Murray, "Consensus problems in networks of agents with switching topology and time-delays," *IEEE Trans. Automat. Control*, vol. 49, no. 9, pp. 1520–1533, Sept. 2004.
[65] R. W. Erickson and D. Maksimovic, *Fundamental of Power Electronics*, 2nd Ed. Norwell, MA: Kluwer, 2001.
[66] D. P. Spanos, R. Olfati-Saber, and R. M. Murray, "Dynamic consensus for mobile networks," in *Proc. 16th Int'l. Fed. Automat. Control (IFAC)*, 2005, pp. 1–6.
[67] L. Chen, C. Hu, Q. Zhang, K. Zhang, and I. Batarseh, "Modeling and triple-loop control of ZVS grid-connected dc/ac converters for three-phase balanced micro-inverter application," *IEEE Trans. Power Electron*, vol. 30, No. 4, pp. 2010–2023, Apr. 2015.
[68] Y. Sozer and D. A. Torrey, "Modeling and control of utility interactive inverters," *IEEE Trans. Power Electron.*, vol. 24, no. 11, pp. 2475–2483, Nov. 2009.
[69] N. Pogaku, M. Prodanovic, and T. C. Green, "Modeling, analysis and testing of autonomous operation of an inverter-based microgrid," *IEEE Trans. Power Electron.*, vol. 22, no. 2, pp. 613–625, Mar. 2007.
[70] X. Guo, Z. Lu, B. Wang, X. Sun, L. Wang, and J. M. Guerrero, "Dynamic phasors-based modeling and stability analysis of droop-controlled inverters for microgrid applications," *IEEE Trans. Smart Grid*, vol. 5, no. 6, pp. 2980–2987, Nov. 2014.
[71] H. Zhang, F. L. Lewis, and Z. Qu, "Lyapunov, adaptive, and optimal design techniques for cooperative systems on directed communication graphs," *IEEE Trans. Ind. Electron.*, vol. 59, no. 7, pp. 3026–3041, Jul. 2012.
[72] F. Xiao and L. Wang, "Asynchronous consensus in continuous-time multi-agent systems with switching topology and time-varying delays," *IEEE Trans. Automat. Control*, vol. 53, no. 8, pp. 1804–1816, Sept. 2008.
[73] S. Ci, J. Qian, D. Wu, and A. Keyhani, "Impact of wireless communication delay on load sharing among distributed generation systems through smart microgrids," *IEEE Wireless Communications*, vol. 19, no. 3, pp. 24–29, Jun. 2012.
[74] S. Liu, X. Wang, and P. X. Liu, "Impact of communication delays on secondary frequency control in an islanded microgrid," *IEEE Trans. Ind. Electron.*, to be published, DOI: 10.1109/TIE.2014.2367456.
[75] H. Behjati, A. Davoudi, and F. L. Lewis, "Modular DC-DC converters on graphs: cooperative control," *IEEE Trans. Power Electron.*, vol. 29, no. 12, pp. 6725–6741, Dec. 2014.